

Copula Index for Detecting Dependence and Monotonicity between Stochastic Signals

Kiran Karra

*Bradley Department of Electrical and Computer Engineering
Virginia Tech Research Center
Arlington, VA 22033, USA*

KIRAN.KARRA@VT.EDU

Lamine Mili

*Bradley Department of Electrical and Computer Engineering
Virginia Tech
Falls Church, VA 22043, USA*

LMILI@VT.EDU

Abstract

This paper introduces a nonparametric copula-based approach for detecting the strength and uniquely, the monotonicity structure of linear and nonlinear statistical dependence between pairs of random variables or stochastic signals, termed *CIM*. *CIM* satisfies the data processing inequality and is, consequently, a self-equitable metric. Simulation results using synthetic datasets reveal that the *CIM* compares favorably to other state-of-the-art measures of association that satisfy the data processing inequality, including the estimators of mutual information based on k-nearest neighbors, *k-NN*, adaptive partitioning, *AP*, and the von-Mises expansion, *vME*. Additionally, *CIM* performs similarly to other state-of-the-art statistical dependency metrics, including the Maximal Information Coefficient (*MIC*), Randomized Dependency Coefficient (*RDC*), distance correlation (*dCor*), copula correlation (*Ccor*), and the Copula Statistic (*CoS*) in both statistical power and sample size requirements. Simulations using real world data highlight the importance of understanding the monotonicity structure of the dependence.

Keywords: copula, statistical dependency, monotonic, equitability, discrete

1. Introduction

A fundamental problem in statistics and machine learning involves understanding the organization of large datasets and the dependencies between features in them. An unsupervised approach to this problem entails modeling the features within these datasets as random variables and discovering the dependencies and conditional dependencies between them. The most familiar measure of statistical dependence, the correlation coefficient, however only measures linear dependence (Pearson, 1895). Several indices of nonlinear dependence for continuous random variables have been introduced in the literature, including *MIC* (Reshef et al., 2011), the *RDC* (Lopez-Paz et al., 2013), the *dCor* (Székely et al., 2007), the *Ccor* (Chang et al., 2016), and *CoS* (Ben Hassine et al., 2016). *MIC* can process continuous and discrete random variables, but it does so by discretizing continuous random variables. Although heuristics can be applied, finding the optimal discretization algorithm is an NP-complete problem dependent upon the end goals of the data analysis task (García et al., 2013). An additional limitation of these dependence measures is their intrinsic in-

ability to provide a complete insight into the structure of the dependency. By structure, we mean whether the dependency is monotonic or nonmonotonic. One way may be to use the difference between an index of linear dependence such as the correlation coefficient and a nonlinear index of dependence such as *MIC* can be used as a measure of nonlinearity (Reshef et al., 2011). However, this difference cannot fully characterize whether the nonlinearity is monotonic or nonmonotonic. Additionally, this methodology is prone to error, as the measure of nonlinearity must scale identically to the measure of linearity, in order to make sense of any functional operations between these two measures. We show in Section 4.2 that the characterization of the monotonicity structure has important consequences for accurate modeling and analysis of stochastic data.

In this paper, we introduce a new index of nonlinear dependence, termed Copula Index for detecting dependence and Monotonicity, or *CIM* for short. This index is based on copulas and the rank statistic Kendall's τ (Kendall, 1938), that naturally handles continuous, discrete, and hybrid random variables or stochastic signals. In this paper, we define hybrid random variables to be pairs of random variables where one is continuous and the other is discrete. *CIM* identifies nonlinear associations between random variables by transforming realizations of random variables into their pseudo-observations by applying the probability integral transform, scanning them for regions of monotonicity in the dependence structure, and computing a weighted average of association within each of these identified regions. The identified regions of monotonicity, a unique byproduct of the *CIM* algorithm, provide insight into the monotonicity (or lack thereof) between the random variables or stochastic signals. The *CIM* algorithm's ability to identify nonlinear associations as well as the monotonicity characteristics of the dependency for all types of random variables make it a powerful tool for exploratory data analysis.

At a high level, *CIM* overcomes two limitations of Kendall's τ , namely: 1) its inability to handle hybrid random variables and 2) detection of nonmonotonic dependencies. We overcome the first limitation by proposing a new extension to Kendall's τ , which augments its current modifications to account for discrete random variables with a new correction factor for hybrid random variables. We overcome the second limitation by developing a new algorithm to detect regions of monotonicity and processing each region separately.

This paper is organized as follows. Section 2 introduces copulas, rank statistics, and our proposed extension to Kendall's τ . Section 3 then introduces the *CIM* algorithm. Here, important properties of copulas are proved, which theoretically ground *CIM* as an index of dependence. Additionally, properties of the *CIM* index are discussed. Next, section 4 provides simulations to exercise the developed metric against other state-of-the-art dependence metrics, including *MIC*, *RDC*, *dCor*, *Ccor*, and *CoS* and measures of information including *kNN*, *vME*, and *AP* using synthetic data and conducts real-world data experiments with various datasets from the fields of computational biology, climate science, and finance. Concluding remarks are then provided in Section 5.

2. Copulas, Concordance, and Rank Statistics

In this section, we provide a brief overview of copulas, concordance, and rank statistics. We focus on Kendall's τ as it provides the basis for *CIM*, and propose a new extension of

Kendall's τ to account for hybrid random variables. Properties of this extension, denoted τ_{KL} , are then highlighted and discussed.

2.1 Introduction to Copulas and Concordance for Continuous Random Variables

Copulas are multivariate joint probability distribution functions for which the marginal distributions are uniform (Nelsen, 2006). The existence of a copula $C(\cdot)$ associated with a collection of random variables, X_1, \dots, X_n , following a joint probability distribution function, $H(\cdot)$, and marginals $F_{X_i}(x_i)$ is ensured by Sklar's theorem, which states that

$$H(x_1, \dots, x_n) = C(F_{X_1}(x_1), \dots, F_{X_n}(x_n)). \quad (1)$$

This theorem guarantees the unicity of the copula C for continuous random variables and it unveils its major property, which is its ability to capture the unique dependency structure between any continuous marginal distributions X_1, \dots, X_n . Thus, the copula C can be used to define a measure of dependence between continuous random variables.

A popular measure of dependence that is based on the copula is concordance. Concordance is a form of dependence that measures the degree to which two random variables are associated with each other. More precisely, points in \mathbb{R}^2 , (x_i, y_i) and (x_j, y_j) , are concordant if $(x_i - x_j)(y_i - y_j) > 0$ and discordant if $(x_i - x_j)(y_i - y_j) < 0$ (Nelsen, 2006). This can be probabilistically represented by the concordance function, Q , defined as

$$Q = P[(X_1 - X_2)(Y_1 - Y_2) > 0] - P[(X_1 - X_2)(Y_1 - Y_2) < 0] \quad (2)$$

where (X_1, Y_1) and (X_2, Y_2) are independent vectors of continuous random variables with distribution functions H_1 and H_2 having common margins of F (of X_1 and X_2) and G (of Y_1 and Y_2). Nelsen (2006) then shows that the concordance function can be written in terms of the copulas of (X_1, Y_1) and (X_2, Y_2) , C_1 and C_2 respectively, rather than the joint distribution function as

$$Q(C_1, C_2) = 4 \int \int_{\mathbb{T}^2} C_2(u, v) dC_1(u, v) - 1 \quad (3)$$

Note that (3) is the general definition of the concordance between two random vectors (X_1, Y_1) and (X_2, Y_2) with identical marginals but different dependency structures. To compute the concordance between two random variables X and Y , the concordance function in (3) reduces to $Q(C, C)$, where C is the copula of the joint distribution (X, Y) .

Many metrics of association are based on the concept of concordance, with the two most popular being Kendall's τ (Kendall, 1938) and Spearman's ρ (Spearman, 1904). Kendall's τ is defined in terms of the concordance function as

$$\tau = Q(C, C), \quad (4)$$

where C is the copula of the joint distribution (X, Y) , and interpreted as the scaled difference in the probability between concordance and discordance. It can be estimated by

$$\hat{\tau} = \frac{\# \text{ concordant pairs} - \# \text{ discordant pairs}}{\binom{n}{2}}. \quad (5)$$

Concordance-based measures of association such as Kendall's τ are ideal for detecting linear and nonlinear monotonic dependencies because they are rank statistics. These measures have the desirable properties of being margin independent and invariant to strictly monotonic transforms of the data (Scarsini, 1984; Nelsen, 2006).

Although these statistics work well for measuring monotonic association between continuous random variables, adjustments need to be made to account for discrete and hybrid random variables. It turns out that in that case, Sklar's theorem does not guarantee the unicity of the copula C when the marginal distribution functions are non-continuous. If some or all of the marginal distribution functions are associated with discrete random variables, then many copulas satisfy (1) due to ties in the data. Consequently, the measure of concordance becomes margin-dependent (i.e, cannot be expressed solely in terms the joint distribution's copula as in (3)) and in many cases cannot reach 1 or -1 in scenarios of perfect comonotonicity and countermonotonicity, respectively (Genest and Nešlehová, 2007).

2.2 Extension of Kendall's τ for Hybrid Random Variables

Several proposals for adjusting Kendall's τ for ties have been made, including τ_b (Kendall, 1945), τ_{VL} (Vandenhende and Lambert, 2003), and τ_N (Nešlehová, 2007). The common theme among these proposals is that they use different rescaling factors to account for ties in the data. However, even with rescaling, perfect monotone dependence does not always imply $|\tau_b| = 1$, and τ_{VL} is not interpretable as a scaled difference between the probabilities of concordance and discordance (Genest and Nešlehová, 2007). Nešlehová (2007) overcomes both of these limitations and defines the non-continuous version of Kendall's τ , denoted by τ_N as:

$$\tau_N = \frac{4 \int C_{XY}^S dC_{XY}^S - 1}{\sqrt{(1 - E[\Delta F_X(X)])(1 - E[\Delta F_Y(Y)])}}, \quad (6)$$

where C_{XY}^S is the standard extension copula (Schweizer and Sklar, 1974) given by

$$C_{XY}^S(u, v) = (1 - \lambda_1)(1 - \lambda_2)C_{XY}(a_1, a_2) + (1 - \lambda_1)\lambda_2C_{XY}(a_1, b_2) + \lambda_1(1 - \lambda_2)C_{XY}(b_1, a_2) + \lambda_1\lambda_2C_{XY}(b_1, b_2), \quad (7)$$

with

$$\lambda_i = \begin{cases} \frac{u_i - a_i}{b_i - a_i}, & \text{if } a_i < b_i, \forall i = 1, 2, \\ 1, & \text{if } a_i = b_i \end{cases}$$

where a_i and b_i denote the least and the greatest element in the closure of the range of F_X and F_Y such that $a_i \leq u_i \leq b_i \forall i = 1, 2$, and $\Delta F_X(X) = F_X(X) - F_X(X^-)$. Nešlehová (2007) then defines an estimator of the non-continuous version of τ_N as:

$$\hat{\tau}_N = \frac{\# \text{ concordant pairs} - \# \text{ discordant pairs}}{\sqrt{\binom{n}{2} - u} \sqrt{\binom{n}{2} - v}} \quad (8)$$

where $u = \sum_{k=1}^r \binom{u_k}{2}$, $v = \sum_{l=1}^s \binom{v_l}{2}$, r is the number of distinct values observed in x and s is the number of distinct values observed in y , u_k is the number of times the k^{th}

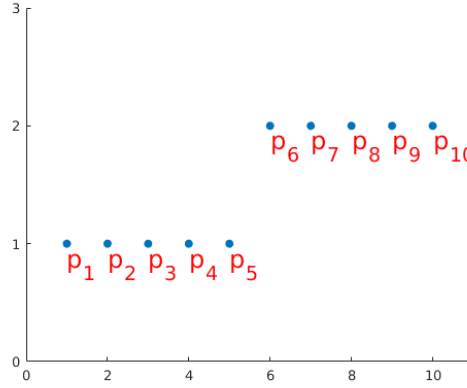


Figure 1: The hybrid random variable pair (X, Y) is comonotonic, with X the continuous random variable and Y the discrete random variable. In the computation of $\hat{\tau}$, the pairs of points $[p_i, p_j]$ for $i = 1 : 5, j = 1 : 5$ and $i = 6 : 10, j = 6 : 10$ are not counted as concordant. Only the pairs of points $[p_i, p_j]$ for $i = 1 : 5, j = 6 : 10$ are, leading to $\hat{\tau}$ not reaching +1 in the perfectly comonotonic case for hybrid random variables.

distinct element occurred in the u dimension, v_l is the number of times the l^{th} distinct element occurred in the v dimension. From (8), it can be seen that $\hat{\tau}_N$ performs well in the discrete case by subtracting the number of ties for each variable u and v independently from the denominator. The subtraction allows the value of $\hat{\tau}_N$ to achieve plus or minus one in the comonotonic and countermonotonic cases, respectively, because ties do not get accounted for in the numerator. The accounting of ties is due to the strict inequalities used for concordance and discordance in (2). In the continuous case, there are no ties and τ_N defined in (6) reduces to the original Kendall's τ defined in (4).

Although the measure defined by (6) is valid for continuous, discrete, or hybrid random variables, the estimator $\hat{\tau}_N$ in (8) does not achieve a value of plus or minus one in the perfectly comonotonic and countermonotonic cases, respectively, for hybrid random variables. In order to extend $\hat{\tau}_N$ to that case, we propose to use the maximum number of ties as a correction factor. This is because in that case, the numerator of $\hat{\tau}_N$ does not count the increasing continuous variables as concordant. Fig. 1 illustrates this counting in an example, and shows why $\hat{\tau}_N$ fails to achieve plus or minus one in the hybrid random variable case for perfectly comonotonic/countermonotonic random variables respectively. In it, the pairs of samples along the continuous dimension x within a discrete value ($[p_i, p_j]$ for $i = 1 : 5, j = 1 : 5$ and $i = 6 : 10, j = 6 : 10$) are not counted as comonotonic. To overcome this drawback, our proposed extension to $\hat{\tau}_N$ is defined as

$$\hat{\tau}_{KL} = \begin{cases} \frac{\# \text{ concordant pairs} - \# \text{ discordant pairs}}{\binom{n}{2}} & \text{continuous} \\ \frac{\# \text{ concordant pairs} - \# \text{ discordant pairs}}{\sqrt{\binom{n}{2}-u}\sqrt{\binom{n}{2}-v}} & \text{discrete} \\ \frac{\# \text{ concordant pairs} - \# \text{ discordant pairs}}{\sqrt{\binom{n}{2}-t}\sqrt{\binom{n}{2}-t}} & \text{hybrid} \end{cases} \quad (9)$$

where $t = \max(u, v) - K$, and where u and v are the same as in $\hat{\tau}_N$, and $K = \binom{u'}{2} \times v'$, u' denotes the number of overlapping points in the continuous dimension and between different discrete values in the discrete dimension, and v' denotes the number of unique elements in the discrete dimension. K is zero for perfectly monotonic hybrid random variables, but takes nonzero values for copula-based dependencies; it helps to reduce the bias of $\hat{\tau}_{KL}$ when hybrid random variable samples are drawn from a copula dependency. The expression of $\hat{\tau}_{KL}$ given by (9) can be interpreted as the scaled difference between $P[(X_1 - X_2)(Y_1 - Y_2) > 0]$ and $P[(X_1 - X_2)(Y_1 - Y_2) < 0]$, which yields under $H_0 : X \perp\!\!\!\perp Y$, $P[(X_1 - X_2)(Y_1 - Y_2) > 0] - [(X_1 - X_2)(Y_1 - Y_2) < 0] = 0$ by definition of concordance. Thus, regardless of the scaling factor, $E[\hat{\tau}_{KL}]$ will be zero when $X \perp\!\!\!\perp Y$.

Figs. 2 (a),(b),(c), and (d) show the bias and variance between the estimated value of $\hat{\tau}_{KL}$ and the value of τ that generates the corresponding copula. Here, samples of $X = F_X^{-1}(U)$ and $Y = F_Y^{-1}(V)$ are drawn from a Gaussian distribution and from a uniform discrete distribution, respectively. All the samples are generated using four possible copulas averaged over 300 Monte-Carlo simulations; U and V are generated by drawing pseudo-observations from the copula model. This follows the methodology described by Madsen and Birkes (2013) for simulating dependent discrete data. Figs. 2 (e) and (f) display the bias and variance of $\hat{\tau}_{KL}$ in the comonotonic and countermonotonic cases. The results show that $\hat{\tau}_{KL}$ achieves $+1$ in the comonotonic case for all continuous, all discrete, and hybrid scenarios, and -1 in the countermonotonic case for all continuous, all discrete, and hybrid scenarios. It also achieves low bias and variance among all proposed modifications to estimators of τ for hybrid random variables with copula-based dependencies. The null distribution of $\hat{\tau}_{KL}$ under independence, that is, $X \perp\!\!\!\perp Y$, is depicted in Fig. 3. It shows that $\hat{\tau}_{KL}$ is Gaussian with a mean of approximately zero and a decreasing variance as the sample size M increases for continuous, discrete, and hybrid random variables.

These properties suggest that $\hat{\tau}_{KL}$ can additionally be useful for estimating parametric copulas when building hybrid copula Bayesian Networks (HCBN) (Karra and Mili, 2016), rather than using empirical copulas, which are computationally intractable for large dimensional networks. Briefly, in HCBN, a family of nodes is modeled with a copula; the difficulty that HCBN attempts to address is the scenario where some families contain nodes which are both continuous and discrete. In the context of $\hat{\tau}_{KL}$, when building Hybrid Copula Bayesian networks, families of this nature can be estimated either with parametric copula families, or empirical copulas. Although the latter fit the data with less error, more computational resources are required in order to process inference queries with empirical copulas, rather than parametric copulas with closed form expressions such as the Gaussian or Archimedean families. Thus, for large networks with many nodes, it is preferable to use the parametric copula families; however, using parametric copulas with discrete data is prone to biased estimates (Genest and Nešlehová, 2007). The properties of $\hat{\tau}_{KL}$ shown above suggest that $\hat{\tau}_{KL}$ can be used to estimate a parametric copula's parameter, θ , via the one-to-one relationship between τ and θ that exists for popular copula families, with low bias.

Another example of why the correction factor detailed in (9) is important is displayed in Fig. 4. In it, a step function dependency with various levels of discretization is displayed, and it is seen that with small levels of discretization, $\hat{\tau}_b$ and $\hat{\tau}_N$ misrepresents the dependence

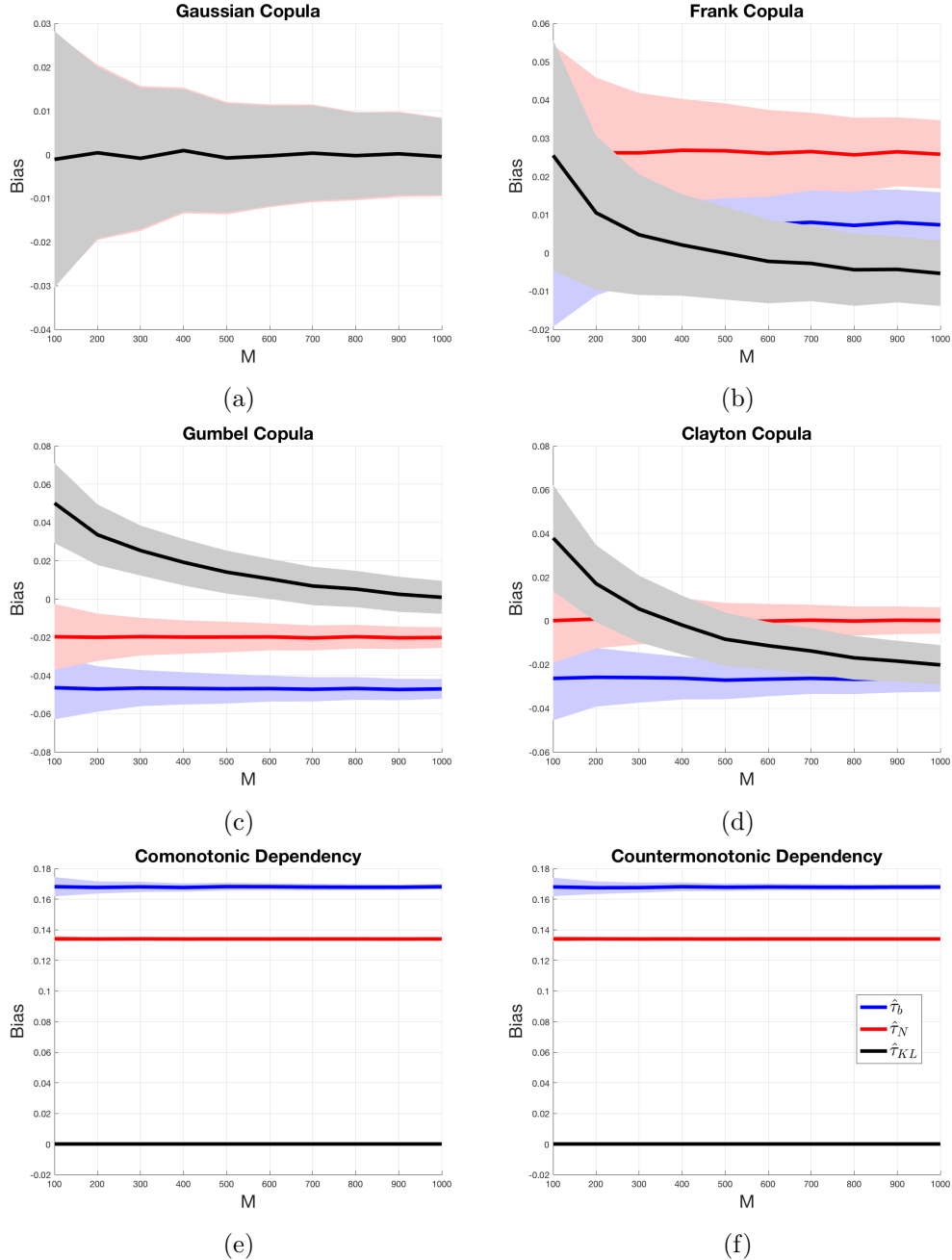


Figure 2: Average bias and standard deviation of $\hat{\tau}_b$, $\hat{\tau}_N$, and $\hat{\tau}_{KL}$ for varying number of samples of copula based and monotonic dependencies with hybrid random variables, where M refers to the sample size. For the copula dependencies, the bias and variance for each sample size was averaged over the entire range of copula dependencies for 300 Monte-Carlo simulations. More specifically, for the Gaussian copula, the copula parameter θ was varied from $[-1, 1]$. For the Frank, Gumbel, and Clayton copulas, the copula parameter α was varied from $[1, 10]$. Samples of $X = F_X^{-1}(U)$ were generated from a normal distribution, and samples of $Y = F_Y^{-1}(V)$ are generated from a uniform discrete distribution and U and V are generated by drawing pseudo-observations from the four possible copula models.

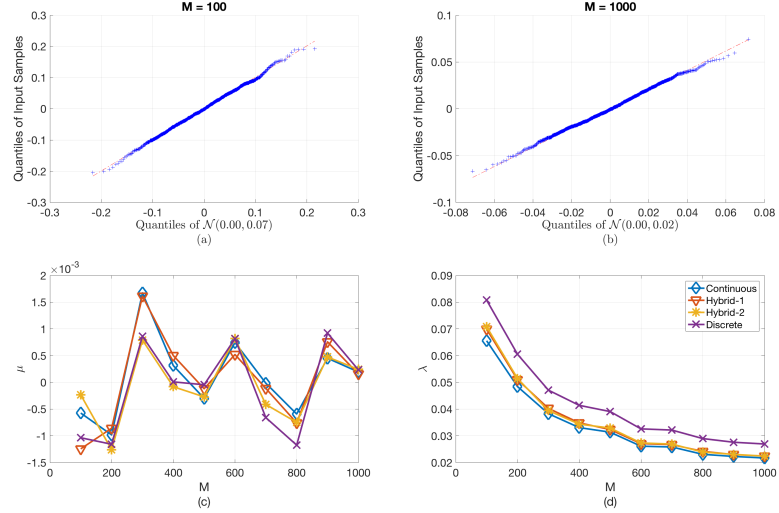


Figure 3: (a) QQ-Plot of $\hat{\tau}_{KL}$ for continuous random variables and X and Y such that $X \perp\!\!\!\perp Y$ and $M = 100$, (b) QQ-Plot of $\hat{\tau}_{KL}$ for continuous random variables X and Y such that $X \perp\!\!\!\perp Y$ and $M = 1000$, (c) The sample mean of the distribution of $\hat{\tau}_{KL}$ for $X \perp\!\!\!\perp Y$ as a function of M (sample size), (d) The sample variance of the distribution of $\hat{\tau}_{KL}$ for $X \perp\!\!\!\perp Y$ as a function of M (sample size). Note: Hybrid-1 refers to a discrete X and continuous Y , Hybrid-2 refers to a continuous X and discrete Y .

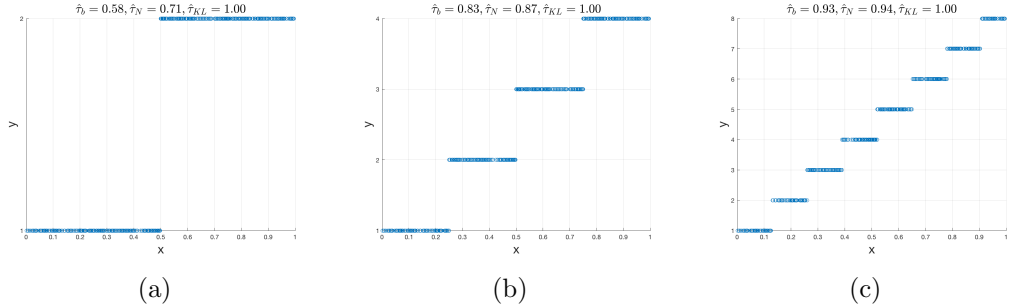


Figure 4: Step function dependency with various levels of discretization; it is seen that τ approaches 1 as the number of discretization levels increases, but without the bias correction described in (9), dependence between continuous and discrete random variables is not measured accurately by τ_b and τ_N .

strength between X and Y , while the correction factor in $\hat{\tau}_{KL}$ compensates and achieves the true dependence value of 1 in all situations.

3. Copula Index for Detecting Dependence and Monotonicity between Stochastic Signals

In this section, we describe how τ_N is used to detect nonlinear monotonic and nonmonotonic statistical dependencies, with a new index termed *CIM*. The theoretical foundations of this

methodology are developed. We then describe the properties of *CIM* and propose an algorithm to estimate it.

3.1 Theoretical Foundations of *CIM*

CIM detects statistical dependencies by leveraging concepts from concordance, defined above in (3). However, measures of association directly based on concordance do not perform well for measuring nonmonotonic dependencies. This is because two random variables can be perfectly dependent, while having the probability of concordance, $P[(X_1 - X_2)(Y_1 - Y_2) > 0]$, equal to the probability of discordance, $P[(X_1 - X_2)(Y_1 - Y_2) < 0]$, yielding a null concordance function Q . One example of such a dependency is $Y = X^2$, with $X \sim U[-1, 1]$. Thus, in order to use concordance as a measure of nonmonotonic dependence, one must consider regions of concordance and discordance separately; this provides the basis of *CIM*. Specifically, *CIM* identifies regions of concordance and discordance, and computes a weighted average of $|\tau_{KL}|$ for each of these regions.

To develop the *CIM*, we begin by proving that a set of observations drawn from any mapping can be grouped into concordant and discordant subsets of pseudo-observations which are piecewise linear functions of each other. Let $F_{X_d}(x_d(m))$ is the m^{th} pseudo-observation for the d^{th} dimensional data point and denote the range-space of (X, Y) , where X and Y are random variables, to be the subset of \mathcal{R}^2 which encompasses every pair of values that the bivariate random variable (X, Y) can take on. Based on these definitions, we can state the following theorem:

Theorem 1 *Suppose X and Y are random variables where X and Y are associated through the mapping defined by $g(\cdot)$, where $g(\cdot)$ is monotone over each of the regions $\Omega_i \forall i = 1, \dots, n$ that form a partition of the range-space of (X, Y) . Define the random variables $U = F_X(x)$ and $V = F_Y(y)$. Then, V is a piecewise linear function of U .*

See Appendix A for the proof.

Theorem 1 shows that if two random variables are dependent in a deterministic sense, their Cumulative Distribution Functions (CDFs) are piecewise linear functions of each other. This implies that the pseudo-observations of realizations of these dependent random variables can be grouped into regions of concordance and discordance. Furthermore, in each region, the dependent variable's pseudo-observations are linear functions of the independent ones, contained in the unit square \mathbf{I}^2 . Using this as a basis, *CIM* detects dependencies by identifying regions of concordance and discordance after transforming the original data x and y into pseudo-observations, $F_X(x)$ and $F_Y(y)$ respectively.

As displayed in Fig. 5a, by definition of concordance, in the independence scenario, no regions of concordance or discordance exist. Similarly, as depicted in Fig. 5b, for monotonic dependencies only one region, \mathbf{I}^2 , exists. Finally, for nonmonotonic dependencies, many regions may exist. As an example, Fig. 5c displays the pseudo-observations of sinusoidal functional dependence. Here, it is easy to see that R_1 and R_3 are regions of concordance, and R_2 is a region of discordance.

The foregoing examples motivate the following definition of the *CIM*:

$$CIM = \sum_i (w_i |\tau_N^i|), \quad (10)$$

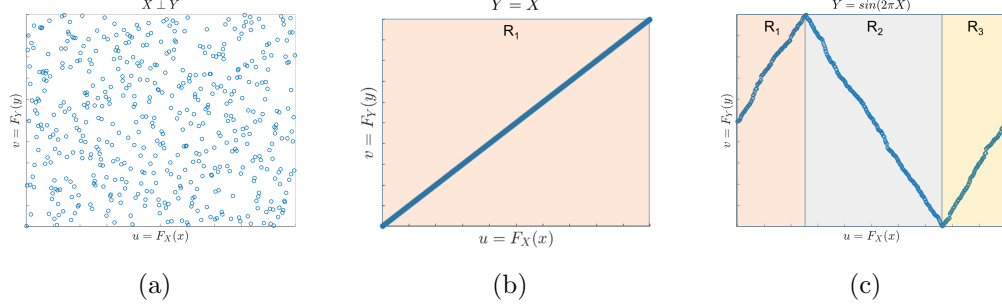


Figure 5: Regions of concordance and discordance for three different scenarios: (a) shows two independent random variables, in which case by definition there are no regions of concordance or discordance; (b) shows comonotonic random variables, in which there is one region of concordance, R_1 ; (c) shows a sinusoidal dependence between two random variables, in which there are two regions of concordance, R_1 and R_3 , and one region of discordance, R_2 .

where $|\tau_N^i|$ is the absolute value of (6) for the i^{th} region and w_i is the ratio of the area of region R_i to \mathbf{I}^2 . From (10) and the properties of τ_N , CIM reduces to τ for monotonic continuous random variables, and zero for independent random variables. It should be noted that (10) defines the CIM metric, but an algorithm is required in order to identify each region for which τ_N is computed. In Section 3.3, we propose an algorithm to identify these regions.

3.2 Properties of CIM

In this section, we describe the properties of CIM . We begin by discussing Rényi's seven properties of dependence measures, and show that CIM satisfies six of them. We then discuss the metric's characteristics and properties under noise, and show through simulations and the definition of concordance, that any dependency metric based on concordance (including CIM) does not follow Reshef's definition of equitability, known as R^2 -equitability. We then show that CIM does, however, satisfy the Data Processing Inequality (DPI), which implies that it satisfies self-equitability. We now discuss the implications of this property for the CIM metric.

3.2.1 DEPENDENCE METRIC PROPERTIES

Alfréd Rényi defined seven desirable properties of a measure of dependence, $\rho^*(X, Y)$, between two random variables X and Y (Rényi, 1959):

1. $\rho^*(X, Y)$ is defined for any pair of non-constant random variables X and Y .
2. $\rho^*(X, Y) = \rho^*(Y, X)$.
3. $0 \leq \rho^*(X, Y) \leq 1$.
4. $\rho^*(X, Y) = 0$ iff $X \perp\!\!\!\perp Y$.

5. For bijective Borel-measurable functions, $f, g: \mathbb{R} \rightarrow \mathbb{R}$, $\rho^*(X, Y) = \rho^*(f(X), g(Y))$.
6. $\rho^*(X, Y) = 1$ if for Borel-measurable functions f or g , $Y = f(X)$ or $X = g(Y)$.
7. If $(X, Y) \sim \mathcal{N}(\mu, \Sigma)$, then, $\rho^*(X, Y) = |\rho(X, Y)|$, where ρ is the correlation coefficient.

CIM satisfies the first property because it operates on copula transformed data (pseudo-observations, which exist for any random variable) rather than the raw data. Because of the following identities: $\sum_i w_i = 1$, $\min(|\tau_N^i|) = 0$, and $\max(|\tau_N^i|) = 1$, the value of *CIM* given by (10) takes values between 0 and 1, and thus the third property is satisfied. In the independence case, because there are no regions of concordance or discordance, (10) reduces to $|\tau_N| = 0$. From Scarsini (1984), any measure of concordance is 0 when X and Y are independent; because *CIM* reduces to $|\tau_N|$, which is an absolute value of the concordance measure τ for independent random variables, the fourth property is satisfied. The fifth property is satisfied because Kendall's τ is invariant to increasing or decreasing transforms (see Nelsen, 2006, Theorem 5.1.8), so the convex sum of Kendall's τ must also be invariant to increasing or decreasing transforms. Note that we cannot guarantee that τ_N be invariant to bijective transforms because the rescaling depends upon the marginal distributions. Thus, the fifth property is only valid for *CIM* for continuous random variables. The second and sixth properties are satisfied by virtue of Theorem 1. Finally, although the seventh property is not directly satisfied by *CIM*, if $(X, Y) \sim \mathcal{N}(\mu, \Sigma)$, the *CIM* metric is the absolute value of Kendall's τ for a Gaussian copula and can be converted to the correlation coefficient θ , with the relation $\theta = \sin(\frac{CIM\pi}{2})$ in order to satisfy the seventh property. This is because the Gaussian copula captures monotonic linear dependence, and hence there is only one region. Thus, the summation in (10) collapses to $|\tau_N|$, which for continuous random variables is $|\tau|$.

3.2.2 EQUITABILITY AND NOISE PROPERTIES

Equitability is a measure of performance of a statistic under noise. Notionally, an equitable statistic assigns similar scores to equally noisy relationships of different types (Reshef et al., 2011). Kinney and Atwal (2014) formalize this concept as R^2 -equitability. A dependence measure $D[X; Y]$ is R^2 equitable if and only if, when evaluated on a joint probability distribution $p(X, Y)$, that corresponds to a noisy functional relationship between two real random variables X and Y , the relation given by

$$D[X; Y] = g(R^2([f(X); Y])) \quad (11)$$

holds true, where g is a function that does not depend on $p(X, Y)$, R^2 denotes the squared Pearson correlation measure, and f is the function defining the noisy functional relationship $Y = f(X) + \eta$, for some random variable η .

We begin by showing that Kendall's τ , the rank correlation metric which *CIM* is dependent upon, does not satisfy R^2 equitability. The estimator of Kendall's τ is defined in (5), and for a given set n of points in the \mathbb{R}^2 space drawn from random variables X and Y , indexed by a subscript as (x_i, y_i) , computed using

$$\hat{\tau} = \frac{\sum_i^n \sum_j^n \text{sgn}(x_i - x_j) \text{sgn}(y_i - y_j)}{n(n-1)/2} \quad \forall i \neq j, \quad (12)$$

where $sgn(\cdot)$ is the sign function. Equation (12) reveals the lack of equitability. This can be explained as follows. The distance information between points (x_i, y_i) and (x_j, y_j) is not used by the $sgn(\cdot)$ function in (12), and thus, if two different processes generate data where the distances between points vary, then random perturbations to that data (noise) will affect these processes differently from a data ordering perspective, resulting in differing estimates of Kendall's τ .

More concretely, consider the points $p_1 = (0, 0)$, $p_2 = (1, 1)$ and $p_3 = (1, 10)$. It is more likely that the lexicographical ordering between p_1 and p_2 is reversed after the addition of noise, than the ordering between p_1 and p_3 . Fig. 6 shows this phenomenon via simulations. Fig. 6 (a) depicts the noiseless relationship for a uniformly distributed X with the association $Y = X$ is plotted, while Fig. 6 (b) displays the $U = F_X(x)$ and $V = F_Y(y)$, where $Y = X + \mathcal{N}(0, 2)$. As for Fig. 6 (c), it depicts the noiseless relationship for a uniformly distributed X with the association $Y = e^X$, and Fig. 6 (d) displays $U = F_X(x)$ and $V = F_Y(y)$, where $Y = e^X + \mathcal{N}(0, 2)$. Figs. 6 (b) and (d) reveal how the ordering of the data, which directly corresponds to the pseudo-observations, changes when the distance between points is not accounted for. We infer from the plots that the exponential relationship, which generates points that are spaced further apart, is differently affected by noise than the linear relationship. Numerically, Kendall's τ in Fig. 6 (b) is estimated to 0.62, while τ in Fig. 6 (d), it is estimated to 1.0, which again shows that these two processes are differently affected by noise, and thus makes τ an unequitable metric as defined by Reshef et al. (2015).

Additionally, the equitability curves, which show the relationship between τ and R^2 for different relationships, for the two association patterns $Y = X$ and $Y = e^X$ are displayed in Fig. 7. The worst interpretable interval, which can be informally defined as the range of R^2 values corresponding to any one value of the statistic is represented by the red hashed line. Fig. 7 depicts a large interval, which is indicative of the lack of R^2 -equitability of this estimator.

As discussed above, the definition of concordance inherently does not lend itself to the R^2 equitability, which implies that CIM is not an R^2 -equitable statistic. Although equitability is a desirable property, Reshef et al. (2015) show that there exists a direct trade-off between statistical power and equitability. We empirically validate this trade-off in Section 4.1.

3.2.3 SELF EQUITABILITY AND THE DATA PROCESSING INEQUALITY

Although the R^2 -equitability is difficult to achieve, related properties such as the DPI and self equitability are important desirable properties of a dependence metric. In this section, we prove that $|\hat{\tau}|$ and CIM both satisfy the DPI, and are thus both self-equitable for continuous random variables. We show that the scaling factors proposed in (8) and (9) to account for discrete and continuous random variables, unfortunately, does not satisfy the DPI. We then propose a solution to allow CIM to satisfy DPI, even in the discrete and hybrid scenarios.

The DPI is a concept that stems from information theory. It states that if random variables X , Y , and Z form a Markov chain, denoted by $X \rightarrow Y \rightarrow Z$, then $I(X; Y) > I(X; Z)$, where $I(X; Y)$ is the mutual information between X and Y defined as $I(X; Y) = \int_Y \int_X f_{XY}(x, y) \log \frac{f_{XY}(x, y)}{f_X(x)f_Y(y)} dx dy$, $f_{XY}(x, y)$ is the joint distribution of X and Y , and $f_X(x)$ and $f_Y(y)$ are the marginal distributions of X and Y , respectively (Cover and Thomas,

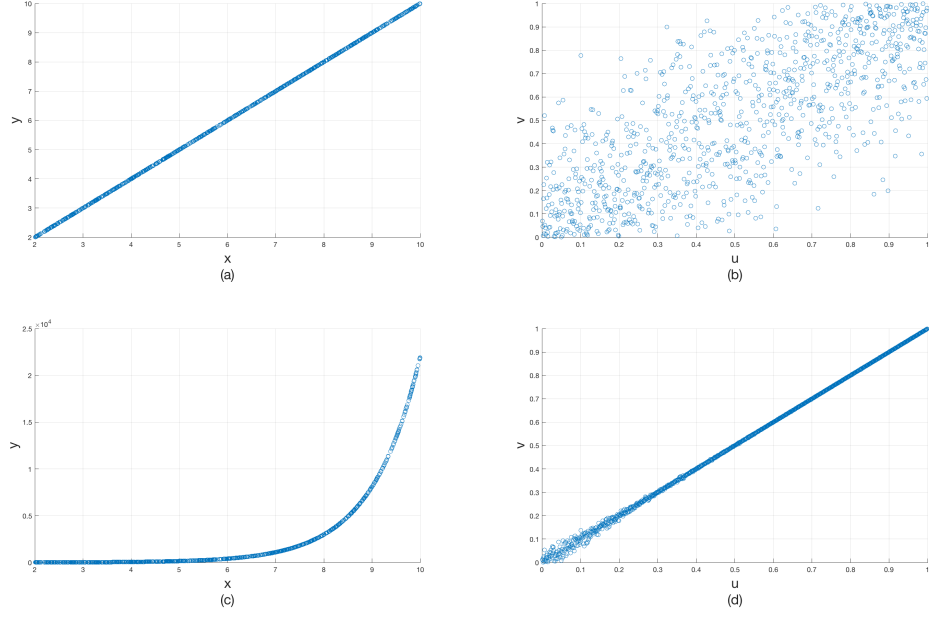


Figure 6: Graphs that show the lack of equitability for concordance. In (a), the dependence $Y = X$ where $X \sim \mathbf{U}(2, 10)$ is shown, while in (b), we show U vs. V , where $U = F_X(x)$ and $V = F_Z(z)$, where $Z = Y + \mathcal{N}(0, 2)$. In (c), the dependence $Y = e^X$ is shown where $X \sim \mathbf{U}(2, 10)$, while in (d), we show U vs. V , where $U = F_X(x)$ and $V = F_Z(z)$, where $Z = Y + \mathcal{N}(0, 2)$. We see that although the same noise was added to both dependencies, the pseudo-observations behave differently. Numerically, τ for the association pattern in (b) is estimated to 0.62, while τ for the association pattern in (d) is estimated to 1.0. However, τ is estimated to be 1 in both (a) and (c). Both (b) and (d) are different functional relationships affected by the same noise, and hence R^2 -equitability is violated by τ .

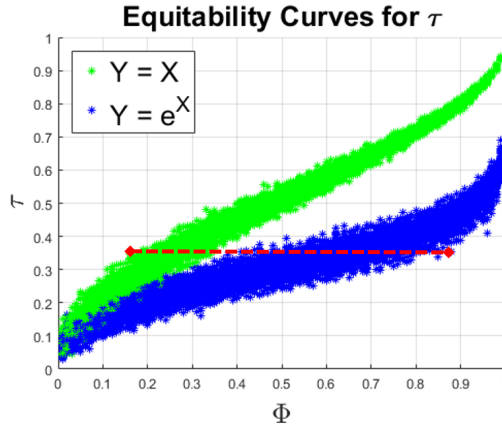


Figure 7: Equitability curves for Kendall's τ for two functional dependencies, where $X \sim U[2, 10]$ and $Y = X$ in green and $Y = e^X$ in blue. Here, we see that the worst interpretable interval, shown by the red hashed line, is large, indicating lack of equitability of $\hat{\tau}$.

2006). Intuitively, it states that information is never gained when being transmitted through a noisy channel (Kinney and Atwal, 2014). As an analog to the information theoretic definition of the DPI, Kinney and Atwal (2014) define a dependence metric D to satisfy the DPI if and only if $D(X; Y) \geq D(X; Z)$, whenever the random variables X , Y , and Z form a Markov chain, $X \rightarrow Y \rightarrow Z$. Here, we prove that CIM , as defined by (10), satisfies the DPI for continuous random variables, and later on we show that a modified version of CIM , termed CIM^S satisfies the DPI for discrete and hybrid random variables. More precisely, we have

Theorem 2 *If the continuous random variables X , Y , and Z form a Markov chain $X \rightarrow Y \rightarrow Z$, then $CIM(X, Y) \geq CIM(X, Z)$.*

See Appendix B for the proof.

An immediate implication of CIM satisfying the DPI is that it can be used for network modeling and information flow of data through Markov chains. One approach is to use the Algorithm for Reconstruction of Accurate Cellular Networks (ARACNe) procedure (Margolin et al., 2006); here, triplets of random variables for which all three CIM values are greater than a baseline threshold are examined, and from the DPI, it can be inferred that no edge exists between the two random variables with the smallest value of CIM (Margolin et al., 2006). Fig. 8 displays a Markov chain of four random variables, $X_1 \rightarrow X_2 \rightarrow X_3 \rightarrow X_4$. In that figure, the network connections between X_1 and X_3 and X_1 and X_4 are represented by red hashed lines (i.e. non-existent connections). This is because from Theorem 2, we infer that $CIM(X_1, X_2) \geq CIM(X_1, X_3)$ and $CIM(X_1, X_2) \geq CIM(X_1, X_4)$. Similar reasoning is applied to the connection between X_2 and X_4 .

Another approach to network modeling using CIM is to perform repeated Max-Relevance Min-Redundancy (MRMR) feature selection (Peng et al., 2005) for each variable in the dataset and construct a Maximum Relevancy Network (MRNET) (Meyer et al., 2007). In principle, for a random variable $X_j \in X$, MRMR works by ranking a set of predictor variables $X_{S_j} \subseteq \{X \setminus X_j\}$ according to the difference between the mutual information (MI) of $X_i \in X_{S_j}$ with X_j (the relevance) and the average MI with the selected variables in X_{S_j} (the redundancy). By choosing the variable that maximizes this difference, a network can be constructed in which direct interactions between variables imply edges. By virtue of Theorem 2, CIM and average CIM can be substituted for MI and average MI to apply CIM to MRNET reconstruction. As for Fig. 8, using the MRNET algorithm and Theorem 2, we can readily say that

$$\begin{aligned} CIM(X_1, X_2) - 0.5[CIM(X_1, X_3) + CIM(X_1, X_4)] &\geq \\ CIM(X_1, X_3) - 0.5[CIM(X_1, X_2) + CIM(X_1, X_4)], \end{aligned}$$

and

$$\begin{aligned} CIM(X_1, X_2) - 0.5[CIM(X_1, X_3) + CIM(X_1, X_4)] &\geq \\ CIM(X_1, X_4) - 0.5[CIM(X_1, X_2) + CIM(X_1, X_3)], \end{aligned}$$

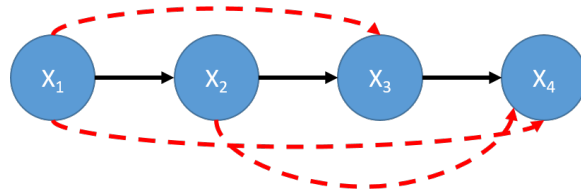


Figure 8: The true Markov Chain $X_1 \rightarrow X_2 \rightarrow X_3 \rightarrow X_4$; because *CIM* satisfies DPI, indirect interactions represented by the red arrows will be removed as edges in the network discovery algorithm for both ARACNe and MRNET.

yielding the connection between X_1 and X_2 in Fig. 8. Similar reasoning can be applied to the other network connections. Simulation results discussed in Section 4.1 motivate the use of *CIM* as a substitute for the *MI*. In it, we compare the statistical power of *CIM* to various estimators of the Mutual Information (MI) including: 1) k -nearest neighbors (k -NN) estimation (Kraskov et al., 2004), 2) adaptive partitioning (AP) MI estimation (Darbellay and Vajda, 1999), and 3) MI estimation via von Mises expansion (*vME*) (Kandasamy et al., 2015), and show that *CIM* is more powerful. This suggests that *CIM* is indeed a viable alternative for use in the estimation of Markov networks from datasets.

Another implication of *CIM* satisfying DPI is that it is a self-equitable statistic. A dependence measure $D(X; Y)$ is said to be self-equitable if and only if it is symmetric, that is, $(D(X; Y) = D(Y; X))$, and satisfies $D(X; Y) = D(f(X); Y)$, whenever f is a deterministic function, X and Y are variables of any type, and $X \rightarrow f(X) \rightarrow Y$ form a Markov chain (Kinney and Atwal, 2014). Self equitability implies that $CIM(X, Y)$ is invariant under arbitrary invertible transformations of X or Y (Kinney and Atwal, 2014), which is in-fact a stronger condition than the 5th property defined by Rényi in his proposed list of desirable properties for dependence metrics (Rényi, 1959).

We now address the case where X , Y , and Z are discrete or hybrid random variables as related to the DPI. Unfortunately, the scaling factors proposed in (8) and (9) to account for discrete and continuous random variables cannot be guaranteed to satisfy the DPI. Indeed, for a Markov Chain $X \rightarrow Y \rightarrow Z$, the scaling factor for $\tau_N(X, Y)$ is $\sqrt{(1 - E[\Delta F_X(X)])(1 - E[\Delta F_Y(Y)])}$. However, the relationship between $E[\Delta F_Y(Y)]$ and $E[\Delta F_Z(Z)]$ is not obvious from $X \rightarrow Y \rightarrow Z$ because the scaling factors are dependent on the marginal distributions, which are related to, but not derivable from, knowledge of the joint distribution's copula. Therefore, we cannot infer that $\tau_N(X, Y) \geq \tau_N(X, Z)$. In order to enable *CIM* to satisfy these properties, we propose to remove the scaling factors defined in (9) and to compute $|\hat{\tau}|$ of the standard extension copula given by (7), for both discrete and hybrid random variables (i.e. the numerator in (8) and (9)). More specifically, let us define

$$\tau_S(X, Y) = 4 \int C_{XY}^S dC_{XY}^S - 1,$$

where C_{XY}^S is the standard extension copula expressed by (7). From Denuit and Lambert (2005) and Nešlehová (2007), we know that C_{XY}^S follows the concordance ordering. Combining this property with Theorem 2, it is straightforward to show that $\tau_S(X, Y)$ does

indeed satisfy the DPI, and thus CIM^S defined as

$$CIM^S = \sum_i (w_i |\tau_S^i|), \quad (13)$$

also satisfies the DPI, where w_i is defined as before in (10). The consequences of not using the scaling factor are that τ_S does not reach plus or minus one for either the perfectly comonotonic, or countermonotonic discrete, or hybrid cases. However, from the perspective of ranking dependencies, as long as concordance order is followed, the absolute value of τ_S is irrelevant; only the relative values of $\tau_S(X, Y)$ and $\tau_S(X, Z)$ are pertinent. It should be noted that the effect of the scaling factors is decreased in two scenarios: 1) the support of the discrete random variables is large, and 2) the probability mass is more evenly distributed among the support of the discrete random variable (Genest and Nešlehová, 2007). In these scenarios, it is safe to use CIM as defined in (10) when constructing networks using the DPI principle, as the effect of the scaling factor is negligible in the presence of noisy data. However, in scenarios where the support of the discrete random variables are small, or the discrete distribution is skewed, it is advisable to use (13) when comparing the relative strengths of dependencies for tasks such as building Markov Networks using the ARACNe or MRNET algorithms described above.

3.3 Algorithms

In this section, we propose an algorithm to estimate the CIM metric. From (10), the CIM estimator can be defined as

$$\widehat{CIM} = \sum_i (w_i |\hat{\tau}_{KL}^i|), \quad (14)$$

where $|\hat{\tau}_{KL}^i|$ is the absolute value of (9) for the i^{th} region and w_i is the ratio of the number of samples in R_i to the total number of samples being considered. It is seen that \widehat{CIM} performs a weighted average of $|\hat{\tau}_{KL}|$, computed for each region of concordance and discordance within \mathbf{I}^2 . Thus, the primary goal of the algorithm is to identify these regions of concordance and discordance within \mathbf{I}^2 . To this end, the proposed algorithm performs repeated computations of $\hat{\tau}_{KL}$ on the pseudo-observations of increasing subsets of the data in the unit-square. Large changes in values of $\hat{\tau}_{KL}$ between consecutive subsets of pseudo-observations indicate that a boundary between a concordant and discordant region has been identified. When all the region boundaries have been identified, the CIM value is estimated by applying (14).

More specifically, the first step in approximating the CIM statistic is to transform the data by applying the probability integral transform, via the empirical cumulative distribution function, to both dimensions of the data independently, generating the pseudo-observations. Next, the unit square is scanned to identify regions of concordance and discordance. The output of this step for independent, linear, and sinusoidal association patterns is shown in Figs. 5 (a), (b), and (c) respectively. The scanning is performed by creating an empty region in the unit square, increasing the size of the region by a defined amount, si , in the u dimension, and estimating the $\hat{\tau}_{KL}$ metric over all points contained within that region, denoted by $\hat{\tau}_{KL}$. Every $\hat{\tau}_{KL}$ is compared to the previous value, denoted as $\hat{\tau}'_{KL}$. If

$$\hat{\tau}_{KL} < \hat{\tau}'_{KL} - 4\sigma_{\hat{\tau}_{KL}}, \quad (15)$$

where $\sigma_{\hat{\tau}_{KL}}$ is the standard deviation of the $\hat{\tau}_{KL}$, then a new region boundary is declared. Stated differently, if the current value $\hat{\tau}_{KL}$ has decreased by more than four standard deviations from its previously estimated value $\hat{\tau}'_{KL}$ for the given noise level, then the algorithm declares this a new boundary between monotonic regions.

Fig. 11 pictorially depicts these steps. In Fig. 11 (a), R_1 that has been decided by the algorithm to contain points of concordance, noted by $\hat{\tau}'_{KL}$. Additionally, the green region in Fig. 11 (a) shows the region under consideration by the algorithm, which is an increment of the region by si . $\hat{\tau}'_{KL}$ and $\hat{\tau}_{KL}$ are compared according to the criterion given above. In Fig. 11 (a), the criterion in (15) yields the decision that the points in the green region belong to the same region as R_1 . In Fig. 11 (b), the same criterion in (15) yields the decision that the points in the green region belong to a new region, R_2 , as depicted in Fig. 5c.

The rationale behind this approach can be understood by considering each $\hat{\tau}_{KL}$ as a random variable, with a given mean and standard deviation. For a linear relationship and continuous random variables, a non-parametric view of the distribution of $\hat{\tau}_{KL}$ is shown via box and whisker plots in Fig. 9. In it, it is seen that the variance of $\hat{\tau}_{KL}$ is not only dependent upon the number of samples, but also on the noise level (swept on the x axis). The standard deviation of the $\hat{\tau}_{KL}$ estimate across all noise levels for a linear relationship can be modeled as $\sigma_{\hat{\tau}_{KL}} = (1 - E[\hat{\tau}_{KL}])\text{Var}(\hat{\tau}_{KL})$. This simple model's fit is displayed in Fig. 10, which shows the experimental and predicted value of the standard deviation of $\widehat{\tau_{KL}}$ for various noise levels and sample sizes for a linear relationship. Because each region of monotonicity manifests as a linear relationship after the data is transformed with the probability integral transform, by virtue of Theorem 1, the results from the linear relationship apply to each region of monotonicity independently.

For continuous random variables, because $\hat{\tau}_{KL}$ reduces to $\hat{\tau}$, the standard deviation is analytically characterized as $\frac{2(2M+5)}{9M(M-1)}$, where M is the number of points for which the estimate of $\hat{\tau}_{KL}$ is being computed. For discrete and hybrid random variables, the standard deviation is empirically characterized by using the sample mean in Fig. 3. Because the distribution of $\hat{\tau}_{KL}$ is shown to converge to the Normal distribution, four standard deviations from this value represents a confidence interval associated with a 99.9% probability that the newly added points being tested do not belong to the same region of monotonicity. Thus, the algorithm above can be viewed as a hypothesis testing problem, where the null hypothesis that the next set of points belongs to the same region is rejected at a level of $\alpha = .000063$. By a similar argument, because the standard deviation of the estimate approaches 0 in the limit as $M \rightarrow \infty$, the boundaries of the regions will be perfectly detected in the asymptotic case of an infinite sample size.

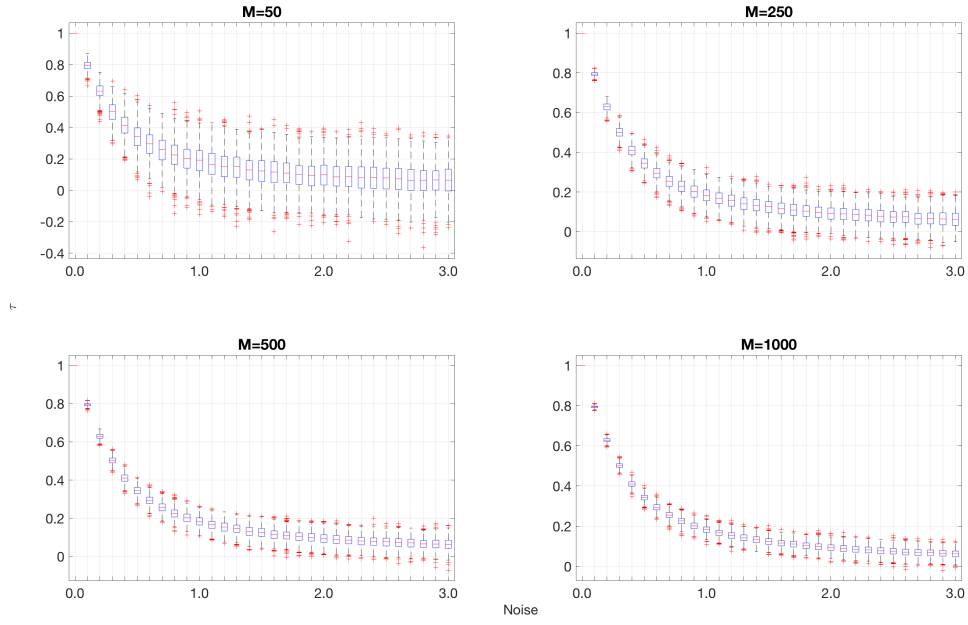


Figure 9: A non-parametric representation of the distribution of $\hat{\tau}_{KL}$ for $y = x + \mathcal{N}(0, \sigma)$, where σ corresponds to the noise level depicted in the x axis of the plot.

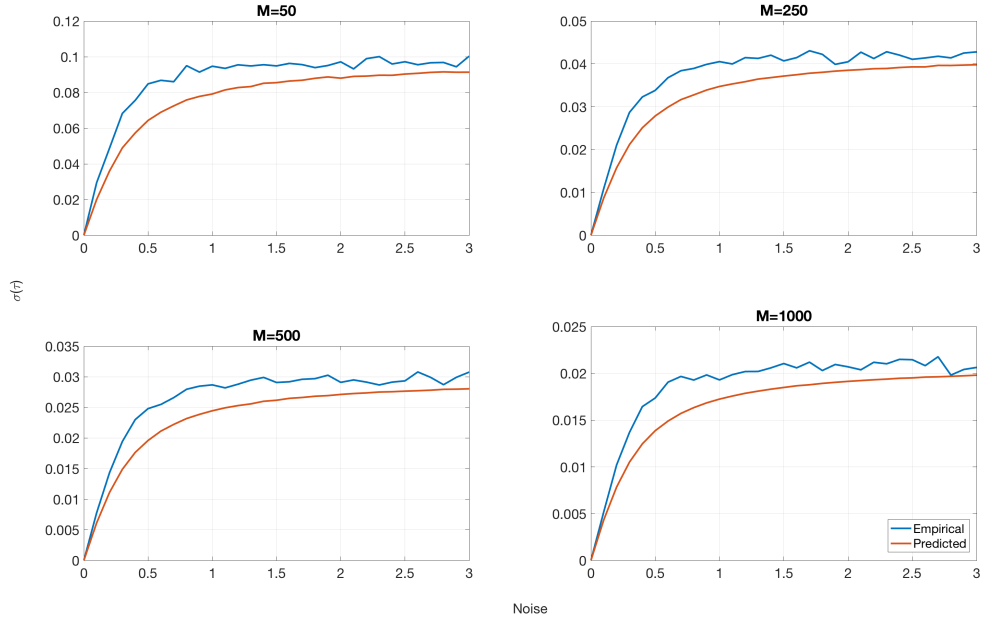


Figure 10: The empirical and predicted values of the standard deviation of $\hat{\tau}_{KL}$ for linear relationship over various noise levels and sample sizes (denoted by M)

Algorithm 1 *CIM*

```

1: function COMPUTE-CIM( $msi$ )
2:    $si \leftarrow [1, \frac{1}{2}, \frac{1}{4}, \frac{1}{8}, \dots, \frac{1}{msi}]$                                  $\triangleright$  Scanning increments to be tested
3:    $uv_{cfg} \leftarrow [u-v, v-u]$                                  $\triangleright$  Orientations of data to be tested
4:    $m_{max} \leftarrow 0, RR \leftarrow []$ 
5:   for  $uv_{cfg}$  in  $uv_{cfg}$  do
6:     for  $si$  in  $si$  do
7:        $\tau, R \leftarrow \text{SCAN-UNIT-SQ}(si, uv_{cfg})$ 
8:        $m \leftarrow 0$ 
9:       for all  $\tau, R$  do                                 $\triangleright$  Compute (10) for detected regions
10:       $n_R \leftarrow \text{GETNUMPOINTS}(R)$ 
11:       $m \leftarrow m + \frac{n_R}{n} \tau_R$ 
12:      if  $m > m_{max}$  then                                 $\triangleright$  Maximize (10) over all scanning increments
13:         $m_{max} \leftarrow m$ 
14:       $RR \leftarrow R$ 
15:   return  $m_{max}, RR$ 
16: function SCAN-UNIT-SQ( $si, uv_{cfg}$ )
17:    $R \leftarrow \text{CREATENEWREGION}$ 
18:    $RR \leftarrow []$ 
19:   while uniqSqNotCovered do
20:      $R \leftarrow \text{EXPANDREGION}(si, uv_{cfg})$                                  $\triangleright$  Expand region by  $si$ 
21:      $m \leftarrow |\tau_{KL}(R)|$                                  $\triangleright |\tau_{KL}|$  of the points encompassed by  $R$ 
22:      $n_R \leftarrow \text{GETNUMPOINTS}(R)$ 
23:      $\sigma_C \leftarrow 4(1-m) \sqrt{\frac{2(2n_R+5)}{9n_R(n_R-1)}}$                                  $\triangleright$  Hypothesis test detection threshold
24:     if  $\neg \text{NEWREGION}(R)$  then
25:       if  $m < (m_{prev} - \sigma_C)$  then
26:          $RR \leftarrow \text{STOREREGION}(R)$ 
27:          $m \leftarrow m$ 
28:        $R \leftarrow \text{CREATENEWREGION}(uv_{cfg})$ 
29:      $m_{prev} \leftarrow m$ 
30:   return  $m, RR$ 

```

`GETNUMPOINTS(R)` - gets the number of points encompassed by the region R

`CREATENEWREGION` - creates a new region of monotonicity from the boundary where the previous region was determined to end

`EXPANDREGION(si, uv_{cfg})` - expands the region by the scanning increment amount, si , as depicted in Fig. 11 in the orientation specified by the uv_{cfg}

`STOREREGION(R)` - called when a boundary between regions is detected; stores the region R 's boundaries and the value of $|\tau_{KL}|$ for this region.

`NEWREGION(R)` - determines if the region R was created in the last loop iteration or not

`UNITSQNOTCOVERED` - a variable which flags when the expansion of R is covering the entire unit square.

Algorithm 1 details a pseudocode description of the proposed algorithm to estimate *CIM* for a given set of configuration parameters. In order to maximize the power of the *CIM* estimator against the null hypothesis that $X \perp\!\!\!\perp Y$, the scanning process described above, and detailed in function `SCAN-UNIT-SQ` of Algorithm 1, is conducted for multiple values of

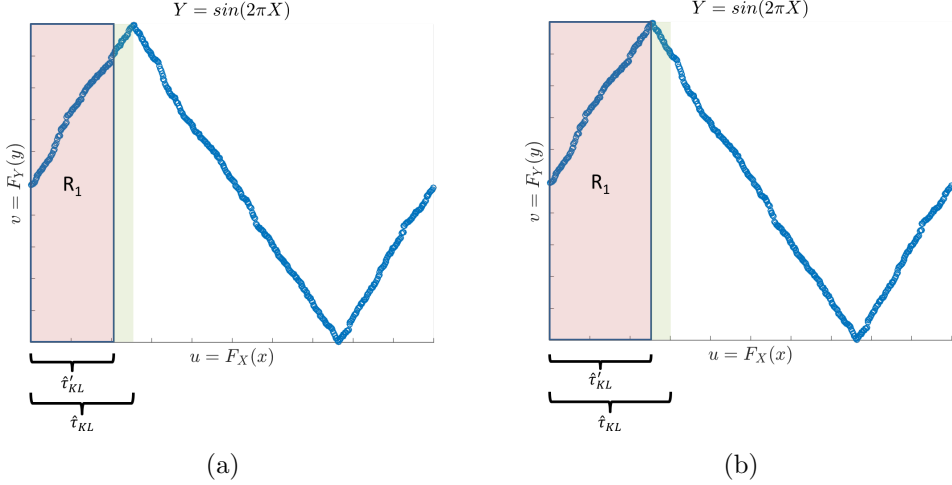


Figure 11: Operation of the *CIM* algorithm. In (a), the *CIM* algorithm decides that the green region belongs to the same region as R_1 . In (b), the *CIM* algorithm decides that green region belongs to a new region, different from R_1 .

si and for both orientations of the unit-square (u-v, and v-u). Line 2 of Algorithm 1 shows that the values of *si* which are tried are a geometrically decreasing series of values in the range of 1 and $\frac{1}{msi}$, where the hyperparameter minimum scanning increment is denoted by *msi*. The choice of using a geometric series to test a series of values between the bounds is arbitrary, and the Algorithm sensitivity testing in Section 3.3.1 leads us to believe that the specific pattern chosen will not have a large effect on the estimated *CIM* value.

The scanning and orientation of the unit square, which maximizes the dependence metric, is the approximate value of *CIM*, as shown in function COMPUTE-CIM. Note that different scanning and orientation values are independent of each other, so the outer two **for** loops in COMPUTE-CIM can be parallelized.

The minimum scanning increment (width of the green region in Fig. 11 (a)), *msi*, is the only hyperparameter for the proposed algorithm. The value of *msi* used in all the simulations, except the sensitivity study, is $\frac{1}{64}$. The denominator of this value bounds the size and frequency of changes to the monotonicity that the algorithm can detect. By choosing $\frac{1}{64}$, it is found that all reasonable dependence structures can be captured and identified. The experiments conducted in Section 4.1 and 4.2 corroborate this choice.

3.3.1 ALGORITHM PERFORMANCE

In this section we investigate the performance of Algorithm 1 using various synthetic datasets. We show that the proposed algorithm is robust to the input hyperparameter. We also investigate the convergence properties and speed of convergence of *CIM* as estimated by Algorithm 1. Because the algorithm performance depends heavily on how well it detects the regions of concordance and discordance, we begin by characterizing the region detection performance.

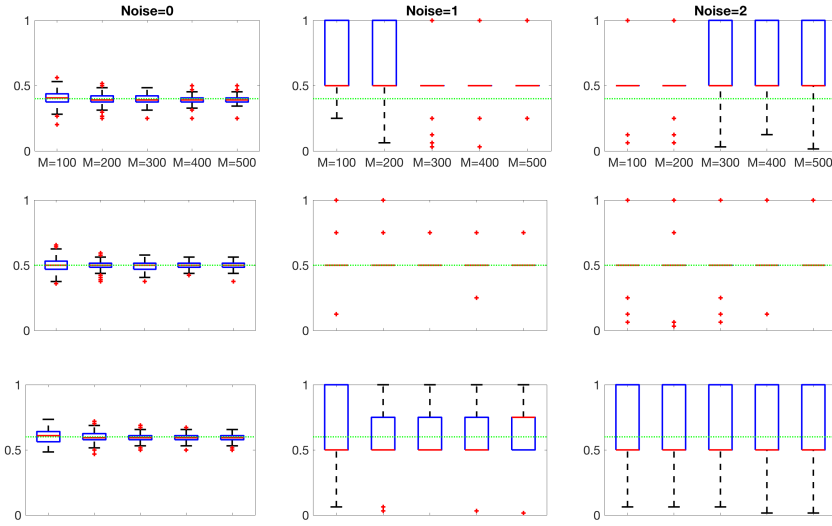


Figure 12: Region boundaries detected by Algorithm 1 for various noise levels and sample sizes. The hashed green line represents the actual region boundary, r , and the box and whisker plots represent the non-parametric distribution of the detected region boundary by Algorithm 1.

To test the region detection performance, we simulate noisy nonmonotonic relationships of the form:

$$Y = 4(X - r)^2 + \mathcal{N}(0, \sigma^2), \quad (16)$$

where $X \sim U(0, 1)$. By varying r and the number of samples, M , that are drawn from X , nonmonotonic relationships of this form comprehensively test the algorithm's ability to detect regions for all types of association. This is because r directly modulates the angle between the two piecewise linear functions at a region boundary, and the number of samples and the noise level test the performance of the decision criterion specified previously in (15) as a function of the number of samples. After generating data according to (16) for various values of r , M , and σ , Algorithm 1 was run on the data and the boundary of the detected region was recorded, for 500 Monte-Carlo simulations. A nonparametric distribution of the detected regions by Algorithm 1 for different values of r and M are displayed in Fig. 12. It is seen that on average, the algorithm correctly identifies the correct region boundary. In the scenario with no noise, the variance of the algorithm's detected region boundary is small, regardless of the sample size. For larger levels of noise, the variance decreases with the sample size, as expected.

Our goal now is to investigate the sensitivity of Algorithm 1 to the hyperparameter msi , for the values $[\frac{1}{4}, \frac{1}{8}, \frac{1}{16}, \frac{1}{32}, \frac{1}{64}]$. For various dependency types, we compute the maximum deviation of the CIM value over 500 Monte-Carlo simulations for sample sizes (M) ranging from 100 to 1000. Fig. 13 shows the maximum deviation of the estimated CIM value for each value of noise over sample sizes ranging from 100 to 1000 for eight different

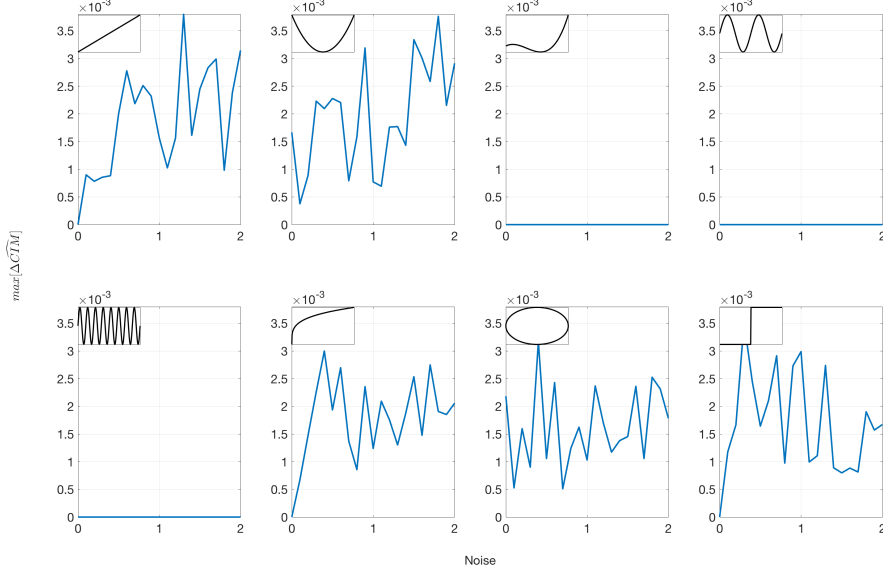


Figure 13: The maximum sensitivity of Algorithm 1 for various association patterns (shown in the upper left inset) swept over different values of noise for sample sizes (M) ranging from 100 to 1000.

association patterns. The results show that the algorithm is robust to different values of the hyperparameter because the maximum deviation of \widehat{CIM} over the noise range, sample sizes, and dependencies tested is no greater than $4e - 3$. In the sensitivity study, we excluded values of msi when testing dependencies for which large values of msi would have masked the dependence structure. For example, in the high-frequency sinusoidal dependency, the monotonicity structure changes at region boundaries with multiples of 0.029. To test the robustness of the algorithm for an msi value of greater than 0.029 does not make sense, so these values were excluded. Similar exclusions were applied to both the cubic and low-frequency sinusoidal dependence structures in the sensitivity tests.

Finally, we show that Algorithm 1 converges to the true CIM value through simulation. The results of the algorithm's convergence performance are shown in Fig. 14 below. The subtitles for each subplot indicate the number of samples required such that the error between \widehat{CIM} and CIM over all computed noise levels is less than 0.01 over 500 Monte-Carlo simulations. It can be seen that for dependencies with small numbers of regions of monotonicity, Algorithm 1 converges very quickly to the true value over all noise levels. For dependencies with large numbers of regions of monotonicity, such as the high frequency sinusoidal relationship depicted in the fifth subplot, a larger number of samples is required in order to ensure convergence. This can be explained from Fig. 9, which shows that the variance of the \widehat{CIM} increases as the number of samples decreases. Thus, with a smaller number of samples in a dependency structure, the increased variance leads Algorithm 1 to make incorrect decisions regarding the region boundaries. As the number of samples increases, the detection performance increases.

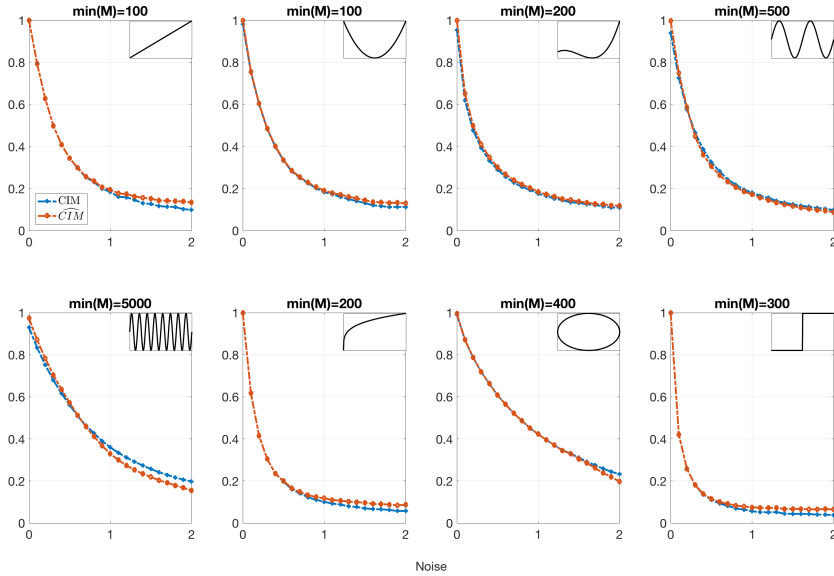


Figure 14: Theoretical and estimated values of CIM for various association patterns shown in the upper right inset swept over different noise levels. The subtitle shows the minimum number of samples for \widehat{CIM} to be within 0.01 of CIM over all noise levels tested for 500 Monte-Carlo simulations.

3.3.2 SAMPLING DISTRIBUTION OF CIM

Simulations were also conducted in order to characterize the null distribution of the CIM approximation algorithm provided in Algorithm 1. It was found experimentally that the the algorithm provided produces a statistic which can be approximated by the Beta distribution, as displayed in Fig. 15. Figs. 15 (c) and (d) both show that as the sample size increases, the α shape parameter remains relatively constant while the β shape parameter increases linearly as a function of M . This roughly corresponds to a distribution converging to a delta function centered at zero. This is a desirable property because it implies that the CIM approximation algorithm yields a value close to 0 for data drawn from independent random variables with a decreasing variance as the number of samples used to compute CIM increases.

It is interesting to note that the Beta distribution is intimately connected to rank statistics. More precisely, one can show that if U_1, \dots, U_n are n independent random variables, each following $\sim U[0, 1]$, then the distribution of the k^{th} order statistic, $U_{(k)}$ follows $\sim \text{Beta}(k, n + 1 - k) \forall k = [1, n]$ (Ahsanullah et al., 2013).

3.3.3 COMPUTATIONAL COMPLEXITY

In this section we describe the computational complexity of computing the CIM algorithm above. We propose a new algorithm to compute $\hat{\tau}_{KL}$ to achieve a computational complexity of $\mathcal{O}(n^2)$ for estimating CIM for continuous and discrete random variables, and $\mathcal{O}(n^3)$ for hybrid random variables.

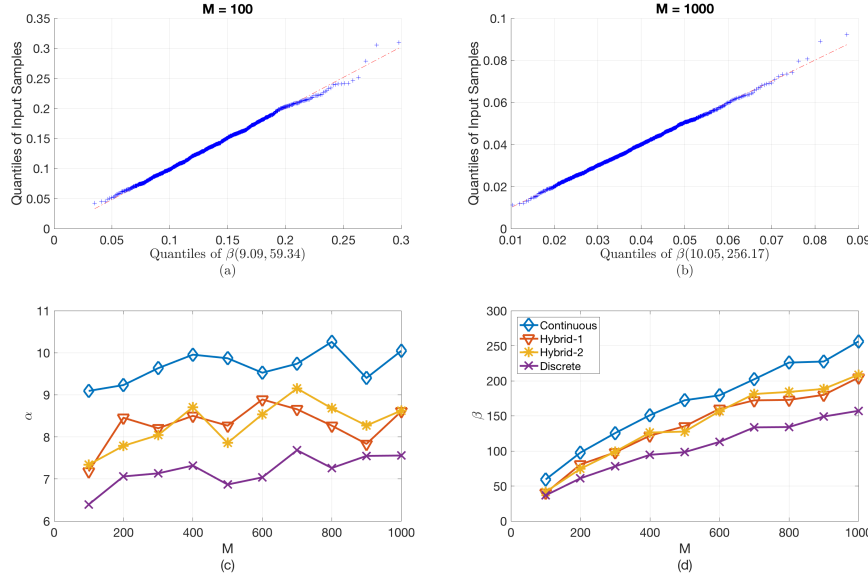


Figure 15: (a) QQ-Plot of CIM for continuous random variables X and Y such that $X \perp\!\!\!\perp Y$ and $M = 100$, (b) QQ-Plot of CIM for continuous random variables X and Y such that $X \perp\!\!\!\perp Y$ and $M = 1000$, (c) α of the distribution of CIM as a function of M , (d) β of the distribution of CIM as a function of M

The core of Algorithm 1 consists of repeated computations of $\hat{\tau}_{KL}$. If one were to naïvely compute this, by recomputing the number of concordant and discordant pairs every time a new region was tested, the operations required to compute the number of concordant and discordant samples would exponentially increase. Instead, we describe an algorithm to compute $\hat{\tau}_{KL}$ efficiently while accumulating new samples into the batch of data for which the value of $\hat{\tau}_{KL}$ is desired (i.e. when expanding the region by si). The essence of the algorithm is that it pre-sorts the data in the direction being scanned, so that the number of concordant and discordant samples do not need to be recomputed in every iteration of the scanning process. Instead, the sorted data allows us to store in memory the number of concordant and discordant samples, and update this value every time a new sample is added to the batch of samples being processed. Additionally, during the sorting process, the algorithm converts floating point data to integer data by storing the statistical ranks of the data rather than the data itself, allowing for potentially efficient FPGA based implementations. The efficient algorithm to compute $\hat{\tau}_{KL}$ for continuous and discrete data, given a new sample, is described in the `CONSUME` function of Algorithm 2. If n samples are to be processed, then the `CONSUME` function is called n times. For clarity of exposition, the remaining helper functions are not presented; however, their operation is only to initialize the variables.

The `CONSUME` function has a computational complexity of $\mathcal{O}(n)$, due to lines 9 and 10 in Algorithm 2, which require computation over a vector of data. Because the `consume` function is called n times in order to process all the samples, this algorithm has a computational complexity of $\mathcal{O}(n^2)$. It should be noted that lines 9 and 10 in Algorithm 2 are vectorizable operations, and the initial presorting is an $\mathcal{O}(n \log(n))$ operation. For hybrid data, addi-

tional calculations are required in the `CONSUME` function in order to count the number of overlapping samples between discrete outcomes in the continuous domain, as described in (9). This requires an additional $\mathcal{O}(n)$ operations, bringing the computational complexity to process hybrid random variables to $\mathcal{O}(n^3)$. For clarity, the pseudocode to compute the overlapping points is not shown in Algorithm 2, but a reference implementation to compute $\hat{\tau}_{KL}$ is provided¹.

¹https://github.com/stochasticresearch/depmeas/blob/master/algorithms/tauKL_s.m

Algorithm 2 τ_{KL}^S

```

1: function CONSUME
2:    $ii_{end} \leftarrow ii_{end} + 1$ 
3:    $mm \leftarrow mm + 1$             $\triangleright$  Increment number of samples, m, we have processed
4:    $mmc2 \leftarrow mmc2 + mm - 1$      $\triangleright$  Increment running value of  $\binom{m}{2}$  for denominator
    $\triangleright$  Get the subset of  $\mathbf{u}$  and  $\mathbf{v}$ 
5:    $\mathbf{u}' \leftarrow \mathbf{u}(ii_{begin} : ii_{end})$ 
6:    $\mathbf{v}' \leftarrow \mathbf{v}(ii_{begin} : ii_{end})$ 
    $\triangleright$  Compute ordering of new sample, in relation to processed samples
7:    $\Delta\mathbf{u} \leftarrow \mathbf{u}'(end) - \mathbf{u}'(end - 1 : -1 : 1)$ 
8:    $\Delta\mathbf{v} \leftarrow \mathbf{v}'(end) - \mathbf{v}'(end - 1 : -1 : 1)$ 
9:    $u^+ \leftarrow \sum [\mathbb{1}(\Delta\mathbf{u} > 0 \cap \Delta\mathbf{v} \neq 0)], u^- \leftarrow \sum [\mathbb{1}(\Delta\mathbf{u} < 0 \cap \Delta\mathbf{v} \neq 0)]$ 
10:   $v^+ \leftarrow \sum [\mathbb{1}(\Delta\mathbf{v} > 0 \cap \Delta\mathbf{u} \neq 0)], v^- \leftarrow \sum [\mathbb{1}(\Delta\mathbf{v} < 0 \cap \Delta\mathbf{u} \neq 0)]$ 
    $\triangleright$  Compute the running numerator,  $K$ , of  $\tau_{KL}$ 
11:  if  $u^+ < u^-$  then
12:     $kk \leftarrow v^- - v^+$ 
13:  else
14:     $kk \leftarrow v^+ - v^-$ 
15:   $K \leftarrow K + kk$ 
    $\triangleright$  Count number of times values in  $u$  and  $v$  get repeated
16:   $\mathbf{uMap}(\mathbf{u}'(end)) \leftarrow \mathbf{uMap}(\mathbf{u}'(end)) + 1, uu \leftarrow uu + \mathbf{uMap}(\mathbf{u}'(end)) - 1$ 
17:   $\mathbf{vMap}(\mathbf{v}'(end)) \leftarrow \mathbf{vMap}(\mathbf{v}'(end)) + 1, vv \leftarrow vv + \mathbf{vMap}(\mathbf{v}'(end)) - 1$ 
    $\triangleright$  Compute threshold for determining if data is hybrid via a threshold heuristic
18:  if  $\neg \text{mod}(mm, OCTZT)$  then
19:     $mmG \leftarrow mmG + 1$ 
20:     $ctzt \leftarrow ctzt + mmG - 1$ 
21:     $uuCtz \leftarrow (uu \leq ctzt)$ 
22:     $vvCtz \leftarrow (vv \leq ctzt)$ 
    $\triangleright$  Compute the denominator of  $\tau_{KL}$  depending on whether data was hybrid or not
23:  if  $(uuCtz \cap vv > 0) \cup (vvCtz \cap uu > 0)$  then
24:     $tt \leftarrow \mathbf{max}(uu, vv)$ 
25:     $den \leftarrow \sqrt{mmc2 - tt} \sqrt{mmc2 - tt}$ 
26:  else
27:     $den \leftarrow \sqrt{mmc2 - uu} \sqrt{mmc2 - vv}$ 
28:  if  $K == 0 \cap den == 0$  then
29:     $\tau_{KL} = 0$ 
30:  else
31:     $\tau_{KL} = \frac{K}{den}$ 
return  $\tau_{KL}$ 

```

4. Simulations

In this section, we compare *CIM* to other metrics of dependence and analyze their performance. We begin by conducting synthetic data experiments to understand the bounds

of performance for all state-of-the-art dependence metrics. We then apply *CIM* to real world datasets from various disciplines of science, including computational biology, climate science, and finance.

4.1 Synthetic Data Simulations

We begin by comparing the estimated indices for various functional and stochastic dependencies for continuous and discrete marginals. The results, displayed in Fig. 16, show that *CIM* performs equivalently to other leading measures of dependence, including MIC_e , RDC , $dCor$, $Ccor$, and CoS for continuous and discrete random variables in the absence of noise. *CIM* achieves $+1$ for all functional dependencies with continuous marginals (Fig. 16 (a), (c)), $+1$ for monotonic functional dependencies with discrete marginals (Fig. 16 (a), (c)), and values close to $+1$ for nonmonotonic functional dependencies with discrete marginals (Fig. 16 (d), (e), (f)). Only RDC shows similar performance. However, as shown in Fig. 16 (b) and (e), RDC has the highest bias in the independence case. We note that discrete random variables were not tested for the $Ccor$ and CoS metrics because the reference implementations were not designed to handle discrete inputs.

Following Simon and Tibshirani (2014), we test the statistical power of the dependence metrics against the null hypothesis that $X \perp\!\!\!\perp Y$. The results in Fig. 17 show that *CIM* displays the best performance for quadratic, cubic, and sinusoidal dependence. For linear, fourth-root, and step function dependence, it performs better than RDC , TIC , and $Ccor$, but is beaten by CoS and $dCor$. In the high frequency sinusoidal case, it is more powerful than the RDC but less powerful than the TIC . This can be explained by the fact that the region configuration which maximizes the dependence (lines 25-26 in Algorithm 1) becomes more ambiguous as the noise level increases when multiple partitions of the range space of $X - Y$ are needed. Our general observations from Fig. 17 are that the CoS and $dCor$ are the best for monotonic dependencies (Fig. 17 (a), 17 (f)), *CIM* exhibits the best performance for small numbers of monotonic regions (Fig. 17 (b), 17 (c), 17 (d)), and TIC performs extremely well for high frequency sinusoidal dependencies (Fig. 17 (e)).

¹The code for these dependency metrics and simulations is provided here: <https://github.com/stochasticresearch/depmeas>, RDC code was adapted from https://github.com/lopezpaz/randomized_dependence_coefficient, $Ccor$ code was ported from <https://github.com/liyi-1989/rcd>, TIC code was adapted from <https://minepy.readthedocs.io/en/latest/>, $dCor$ code was adapted from <https://www.mathworks.com/matlabcentral/fileexchange/49968-dcorr--x--y-->, and CoS code was ported from <https://github.com/stochasticresearch/copulastatistic>

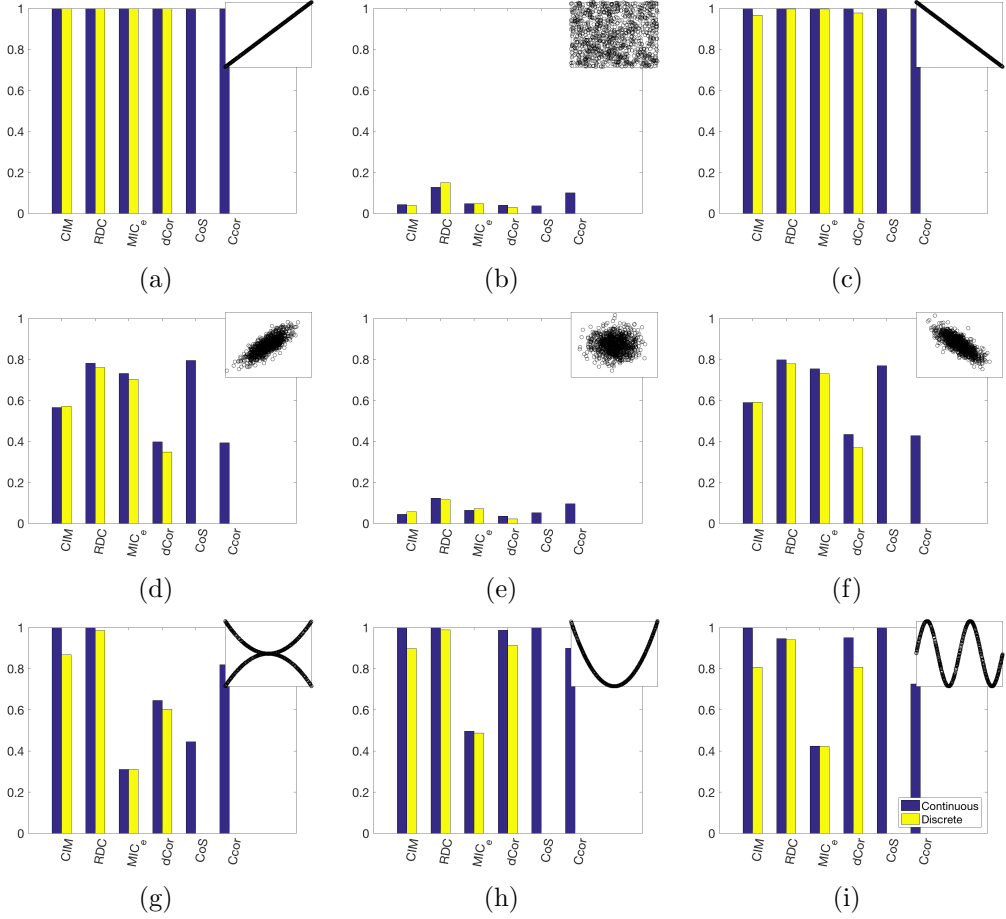


Figure 16: Values attained by various dependence metrics for various noiseless functional associations (a),(c),(g),(h), and (i) and Gaussian copula associations (d), (e), and (f). (b) is the independence case, and (e) is the Gaussian copula with $\rho = 0$.

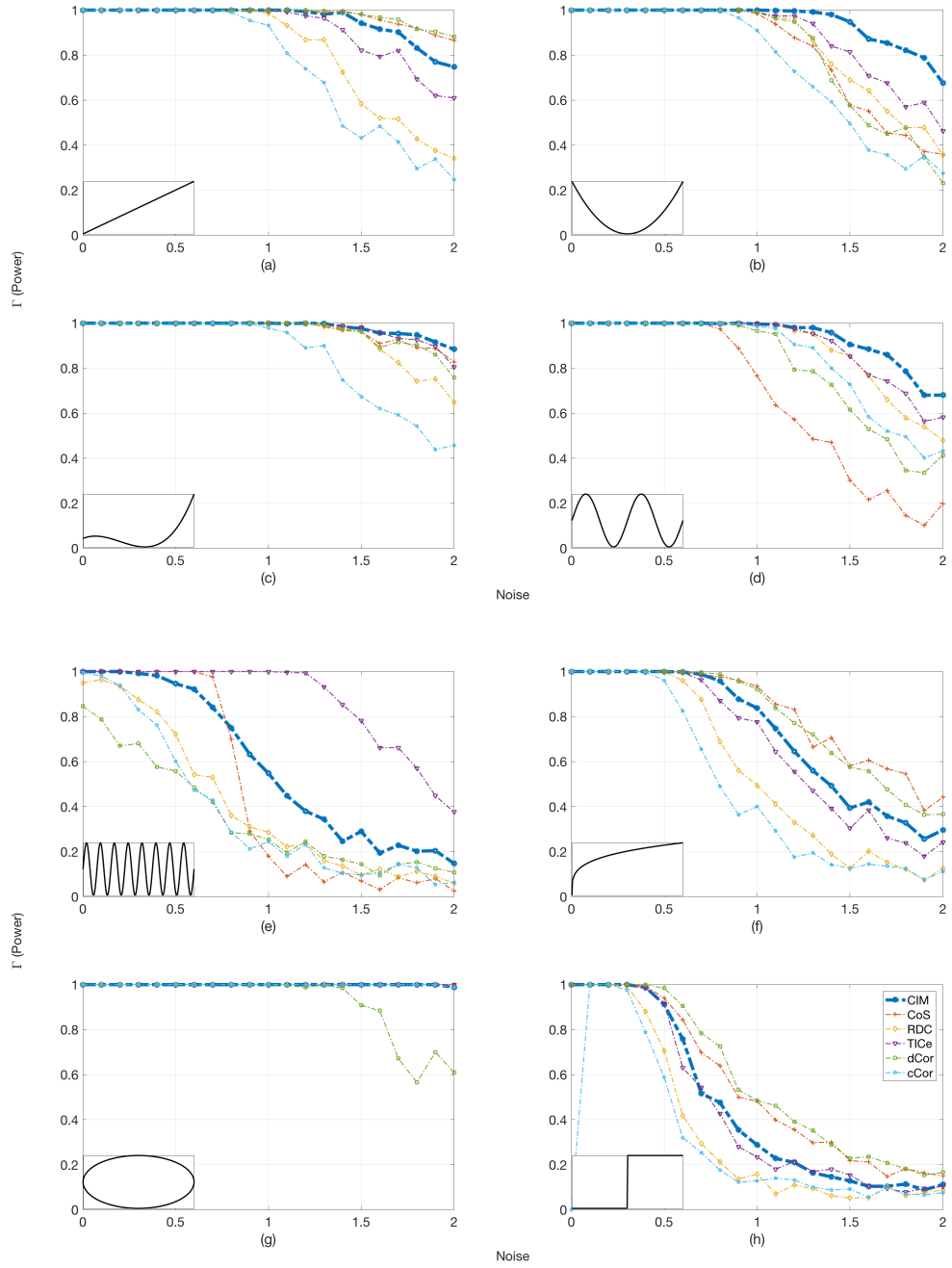


Figure 17: Statistical Power of discussed dependence metrics for several bivariate association patterns as noise increases, for sample size $M = 500$ and computed over 500 Monte-Carlo simulations. Insets show the noise-free form of each association pattern.

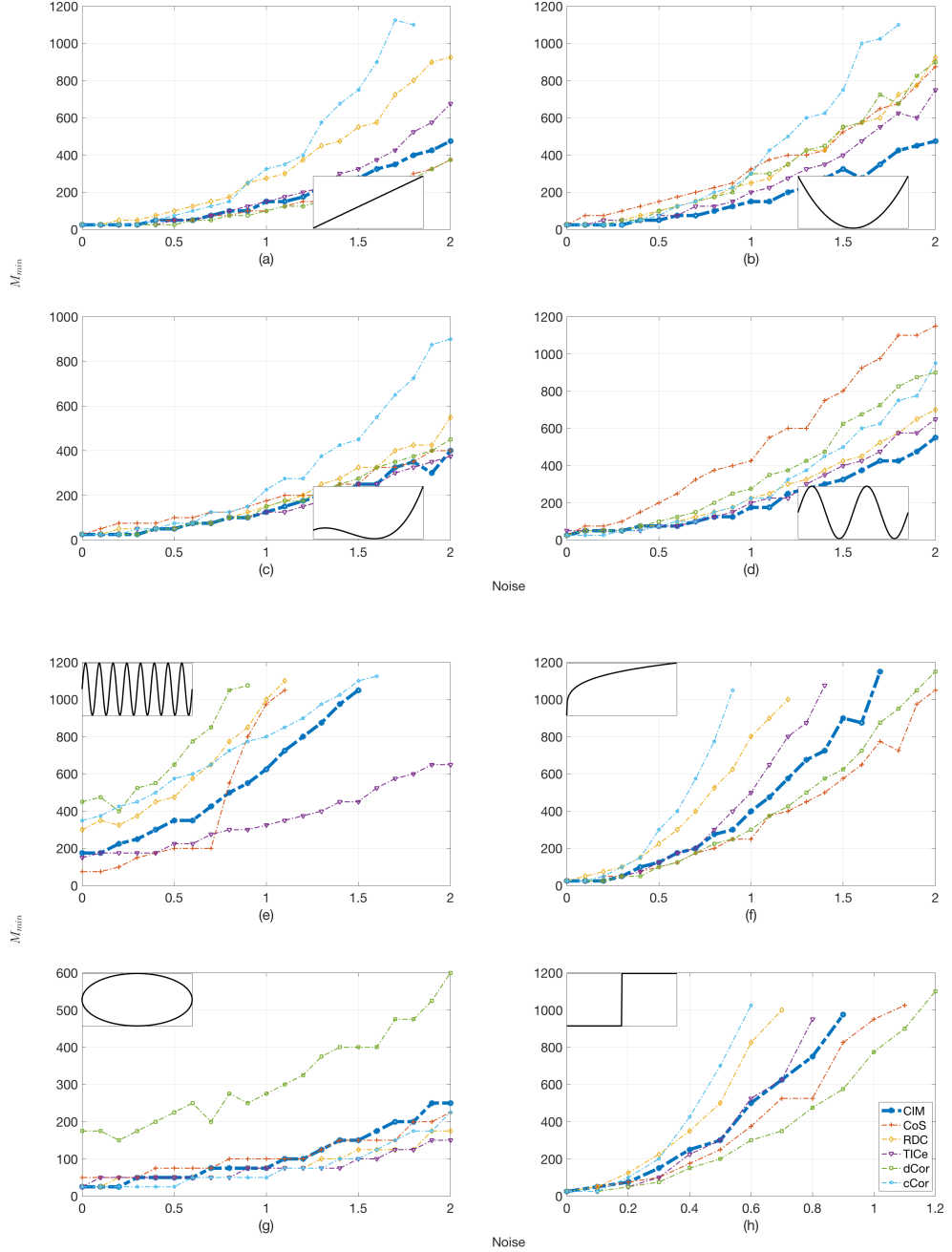


Figure 18: Minimum number of samples required to achieve a statistical power of 0.7 for various association patterns, computed over 500 Monte-Carlo simulations. Inset shows the noise-free form of each association pattern.

We also investigate the power characteristics of the dependency metric as a function of the sample size. Fig. 18 displays the minimum number of samples required to achieve a statistical power of 0.7 for the different dependency metrics for each noise level. The

results show that *CIM* outperforms all other metrics of dependence for dependencies with small numbers of regions of monotonicity, but is beaten by *CoS* and *dCor* for monotonic dependencies. In general, *CIM* displays good small sample performance in general because it is based on Kendall’s τ , which is shown to have superior small sample performance as compared to other metrics of monotonic dependence (Bonett and Wright, 2000; Helsel and Hirsch, 2002).

Finally, we investigate the statistical power of *CIM* against various estimators of Mutual Information, including k-nearest neighbors estimation (Kraskov et al., 2004), adaptive partitioning MI estimation (Darbellay and Vajda, 1999), and MI estimation via von Mises expansion (Kandasamy et al., 2015). The motivation for this simulation stems from Section 3.2.3, where it is suggested that *CIM* be substituted for measures of *MI* when used with network reconstruction algorithms. Fig. 19 compares these metrics and shows that *CIM* outperforms the compared estimators of Mutual Information for the dependency types considered ². The results displayed in Fig. 19 are from simulations with a sample size of $M = 500$. Although we do not include additional plots here, even for small sample sizes such as $M = 100$ (which are typical for biological datasets where estimators of *MI* are commonly used), *CIM* outperforms the compared estimators of *MI* for all the association patterns tested. The results are shown in Figs. 19 (a-h). These experiments suggest that *CIM* can indeed be used in place of estimators of *MI* when used with algorithms which rely on the DPI, such as ARACNe (Margolin et al., 2006) or MRNET (Meyer et al., 2007).

4.2 Real Data Simulations

In this section, we apply the *CIM* metric to real data with the primary goal of characterizing the monotonicity structure of data from different areas of science. This is motivated by the field of joint probabilistic data modeling. More explicitly, for joint probabilistic modeling of large datasets, many copula-based techniques are beginning to be adopted in practice, including Copula Bayesian Networks (Elidan, 2010) and Vine Copula models (Bedford and Cooke, 2002) due to their flexibility and ability to model complex nonlinear relationships between random variables unlike the multivariate Gaussian distribution. The authors of these methods advocate the use of parametric copula families for modeling local joint probability distributions. The main reason for this is that it is computationally efficient to estimate a parametric copula for a joint dataset using the relationship between the copula parameter, θ , and a measure of concordance such as Kendall’s τ . However, popular copula families such as the Archimedean and Gaussian families only capture monotonic dependencies. Thus, if datasets being modeled are nonmonotonic, these copulas will fail to model all the dynamics of the underlying data. Conversely, if the dependencies within these datasets are monotonic, these efficient procedures can be used and data can be fitted to known copula families, and computationally intensive techniques such as estimating empirical copulas can be ignored.

Thus, To know whether a parametric copula family can be used, the monotonicity structure must be understood. Therefore, from a copula modeling and analysis perspective, knowledge of the monotonicity structure provides more actionable information than Reshef’s

²The source code for Shannon Adaptive Partitioning and von Mises based MI estimators is from the ITE Toolbox (Szabó, 2014). K-NN based MI estimation source code is from <https://www.mathworks.com/matlabcentral/fileexchange/50818-kraskov-mutual-information-estimator>

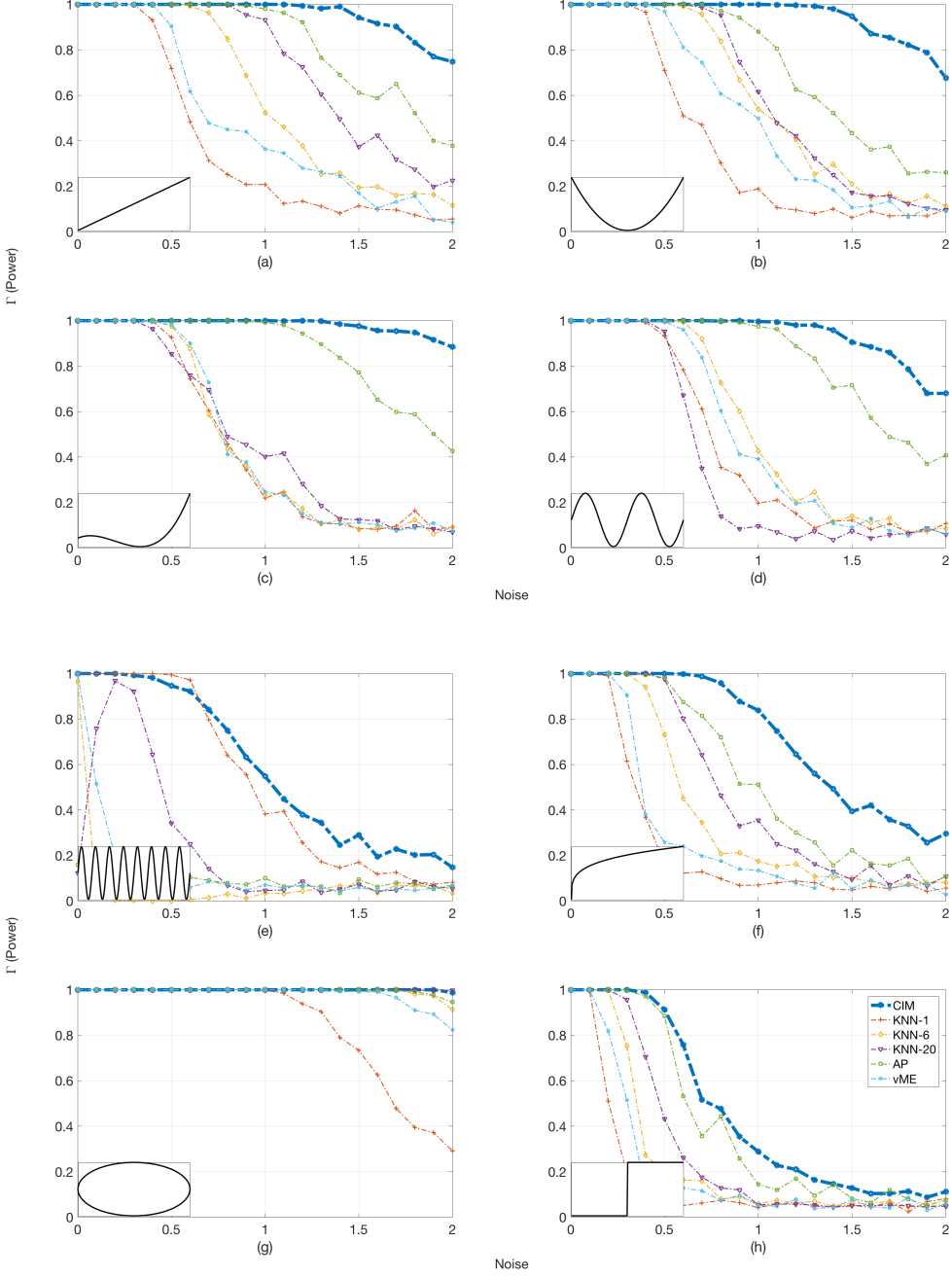


Figure 19: Statistical power of *CIM* and various estimators of mutual information including KNN-1, KNN-6, KNN-20, Adaptive Partitioning, and von Mises Expansion, for sample size $M = 500$ and computed over 500 Monte-Carlo simulations. Inset shows the noise-free form of each association pattern.

proposed nonlinearity coefficient, defined as

$$\theta_{Reshef} = MIC - \rho, \quad (17)$$

where ρ is Pearson's correlation coefficient (Pearson, 1895). Because copulas can capture monotonic nonlinear relationships and the nonlinearity coefficient defined in (17) cannot distinguish between monotonic and nonmonotonic, it is inadequate to answer the probabilistic data modeling question described above.

In order to answer these questions, we processed pairwise dependencies for multiple datasets related to gene expression data, financial returns data, and climate features data³. For each pairwise dependency within a dataset, we count the number of monotonic regions by examining the number of regions detected by the *CIM* estimation algorithm. Additionally, to prevent overfitting, we decide that a pairwise dependency only has one monotonic region if the value of $\hat{\tau}_{KL}$ is within 5 % of the estimated value of *CIM*. When time-series data is compared, we first verify that we only include results of dependencies where the data is considered stationary by the Dickey-Fuller test, at a significance level of $\alpha = 0.05$, and ensure time coherency between the series being compared. Due to the *CIM*'s reliance on copulas, the only requirement is that the data be identically distributed; independence between samples is not required because a copula can capture both inter-dependence as well as serial dependence within realizations of a random variable. Additionally, we only count dependencies if the dependence metric is statistically significant at a level of $\alpha = 0.05$ and the dependence strength exceeds a value of 0.4 as measured by the *CIM* estimation algorithm. Dependencies are only calculated for all unique combinations of features *within* each dataset. With these procedures, after processing 7765 pairwise dependencies which meet the criterion above for various cancer datasets, we found that 96% of gene expression indicators within a cancer dataset are in fact monotonic. Similarly, we process 73 pairwise dependencies between closing price returns data for 30 major indices over a period of 30 years. We found that 99% of the dependencies are monotonic. Finally, we process over 42185 pairwise dependencies of El-Nino indicators in the Pacific ocean, land temperatures of major world cities over the past 200 years, and air quality indicators in major US cities in the past 15 years. In these datasets, termed climate related datasets, we found that 97% of the dependencies within each dataset that meet the criterion above are monotonic. Fig. 20 displays these results, aggregated into pie charts for data analyzed from these diverse areas of science. We are careful to note that the lack of nonmonotonicity in the various datasets that we analyzed is not representative of all real-word datasets.

As stated above, the prevalence of monotonicity in these datasets suggests that techniques that use copula modeling with popular copula families such as the Gaussian or Archimedean families will tend to capture the underlying dynamics of the data properly.

We explore the monotonicity structure thread further in the domain of computational biology by using the *MRNET* algorithm described in Section 3.2.3 with the *MI* estimators previously described, Kendall's τ , and *CIM* using the gene regulatory network benchmarking tool **netbenchmark**. That tool uses over 50 datasets of known gene regulatory networks and compares the performance of a provided algorithm when different amounts of noise are added to the datasets in order to assess in a standardized way, the performance of mutual

³Details of the datasets used and how they were processed are provided in Appendix C

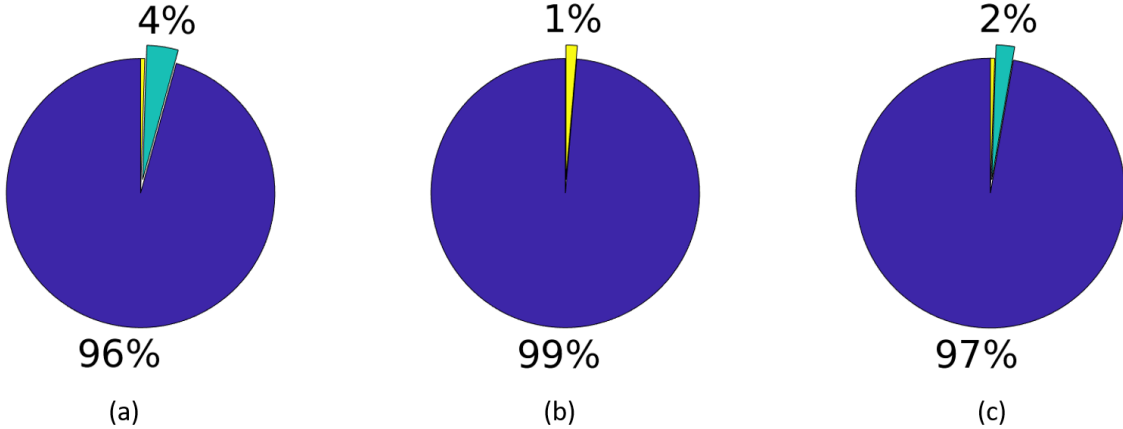


Figure 20: Monotonicity results for various datasets in different areas of science. (a) shows that 96% of the statistically significant dependencies detected in the Gene Expression datasets analyzed had one monotonic region. (b) shows that 99% of the statistically significant dependencies in the financial datasets analyzed had one monotonic region. (c) shows that 97% of the statistically significant dependencies in the climate datasets analyzed had one monotonic region. For all the figures, the blue section of the pie-charts indicates the percentage of statistically significant dependencies which contained one monotonic region. The green section indicates the percentage of significant dependencies which contained two or more monotonic regions.

information based network reconstruction algorithms (Bellot et al., 2015). The datasets used by **netbenchmark** are different than the gene expression datasets we previously analyzed for monotonicity. The area under the precision-recall curve of the 20 most confident predictions (AUPR20) is shown for *MRNET* in Fig. 21, using a measure of monotonic dependence (Kendall’s τ), *CIM*, and the various measures of nonmonotonic dependence using *MI* described previously. The results reveal that for the 150 different variations of the **syntren300** dataset that were compared, the average performance of *MRNET* is actually greater when using *CIM* and τ . These results are not surprising, and are corroborated by the analysis and the results displayed in Figs. 19 and 20 (a). The root cause of this monotonicity needs to be further explored by geneticists and computational biologists.

To study the counter-example of lack of monotonic dependence structures, we examine nonmonotonic dose response data from (Zhu et al., 2013). The data are displayed in Fig. 22, and regions of importance of the relationship between the data as labeled by scientific experts in the field of toxicology is highlighted in the blue and pink regions. Additionally, the unique ability of the *CIM* to identify these regions automatically is shown by the hashed green line. The regions detected by *CIM* correspond to where the monotonicity changes in the dependence structure. Although the regions do not correspond exactly to the regions identified by domain experts (there is no automated way of doing so without expert knowledge of the domain for which the data are being processed), the unique region detection ability of the *CIM* could prove useful in automatically identifying interesting dependence structures for further study by domain experts.

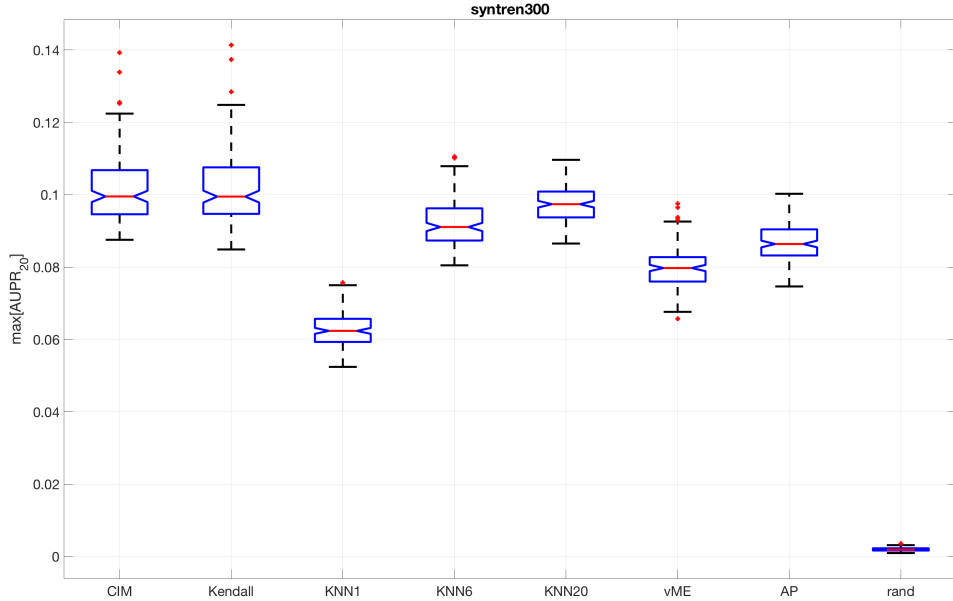


Figure 21: MRNET applied to SYNTREN300 dataset using both measures of monotonic dependence (Kendall and Spearman), and nonmonotonic measures of dependence (MI), for 150 Monte-Carlo simulations.

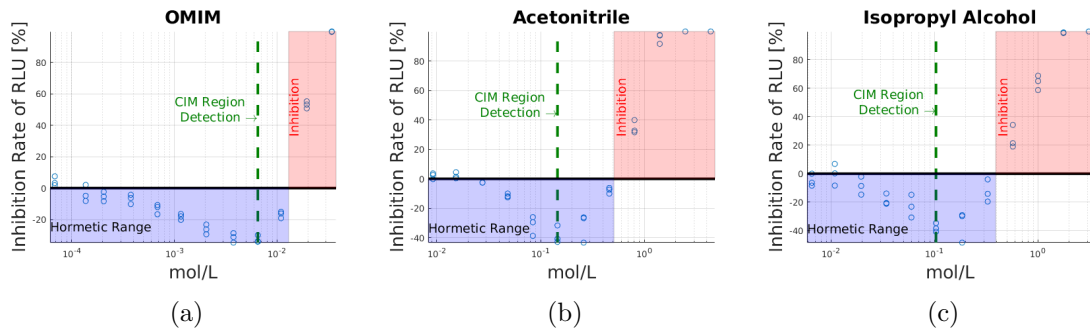


Figure 22: (a) The hormetic effect of 1-octyl-3-methylimidazolium chloride ([OMIM]Cl, CAS RN. 64697-40-1) on firefly luciferase after 15 min exposure (b) the hormetic effect of acetonitrile (CAS RN. 75-05-8) on photobacteria *Vibro-qinghaiensis* sp. Q67 after 15 min exposure, and (c) the hormetic effect of NaBF4 (CAS RN.13755-29-8) on *Vibro-qinghaiensis* sp. Q67 after 12 h exposure. The blue and red regions indicate the hormetic and inhibition regions of the dependence structure, respectively, as indicated by toxicological experts. The green hashed line indicates the region boundary, detected by the *CIM* algorithm.

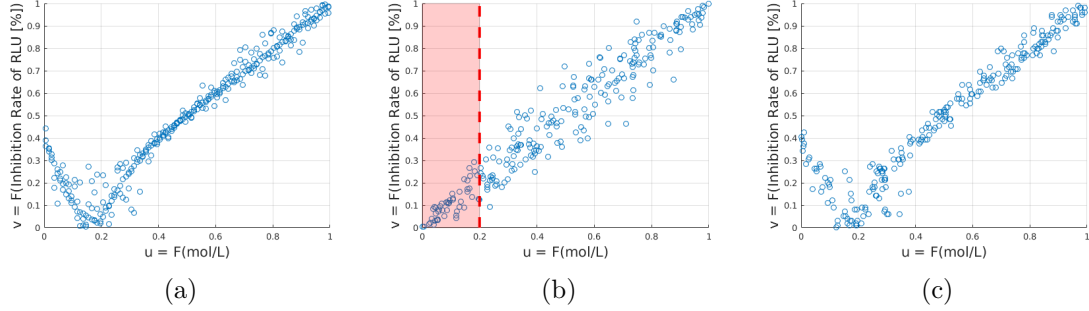


Figure 23: (a) **OMIM** data from Fig. 22a, interpolated with noise to provide more data-points for modeling purposes. (b) Pseudo-Observations of a Gaussian copula model of data in (a). The red highlighted region represents pseudo-observations which are incorrectly modeled by the Gaussian copula model. (c) Pseudo-Observations of an empirical copula model of data in (a).

To understand why regions of monotonicity are important to understand from a data modeling perspective, we take the **OMIM** data from Fig. 22a and show the difference between modeling it with a Gaussian copula and an empirical copula. Fig. 23b shows pseudo-observations drawn from a Gaussian copula model of the data displayed in Fig. 22a, and Fig. 23c shows the pseudo-observations drawn from an empirical copula model of the data displayed in Fig. 22a. The red highlighted region represents pseudo-observations which are incorrectly modeled by the Gaussian copula model. This problem would in fact occur with any popular copula model, including copulas from the Archimedean family, due to the fact that the latter only capture monotonic dependence structures.

We conclude by recognizing that although generalizations about all datasets cannot be drawn from these findings, it is prudent to understand the details of the dataset being analyzed. More specifically, in the context of assessing dependency and modeling joint behavior probabilistically, the simulations conducted show the importance of understanding whether dependencies are monotonic or not.

5. Conclusions and Future Work

In this paper, we described a new statistic of dependence between discrete, hybrid, and continuous random variables and stochastic signals termed *CIM*, based on copula theory. We showed that this index follows six out of the seven Rényi's properties for a metric of dependence, satisfies the data processing inequality (DPI), and is a self-equitable metric. The implications of satisfying DPI are then discussed in the context of construction of Markov networks using DPI measures. *CIM* is then compared to other measures of mutual information and state-of-the-art nonparametric measures of dependence, and is shown to compare favorably and similarly to these compared metrics in various synthetic data experiments. A unique output of the *CIM* estimation algorithm is the number of regions of monotonicity in the dependence structure. This information is used to analyze numerous real world datasets. The results revealed that among all the datasets compared, atleast 96% of the statistically significant dependencies are indeed monotonic. Due to the tradeoff

between statistical power and detecting nonmonotonic dependencies, it is somewhat unanticipated to find that using monotonic measures of dependence (Kendall's τ) rather than nonmonotonic measures (Mutual Information) network modeling applied to Gene Regulatory networks yield a better area under the precision-recall (AUPR) metric. Although generalizations about the monotonicity of all data sources and dependence structures cannot be made, simulations conducted with real-world datasets highlight the need to fully understand the dependence structure before applying statistical techniques.

In its current form, *CIM* is a powerful tool for bivariate data analysis. However, there are many directions to further this research. A logical first step is to extend *CIM* to a measure of multivariate dependence. To accomplish this, it is important to understand how monotonicity is defined in the multivariate Euclidean space, and how to detect these regions of monotonicity, whether that be directly through a scanning algorithm as was proposed in Algorithm 1 or other means such as projection methods. After algorithms are developed to efficiently and accurately detect these regions, multivariate measures of Kendall's τ such as the proposal made by Joe (1990) can be substituted to create the multivariate version of *CIM*. Along the algorithm design thread, additional research can be conducted to improve the performance of the *CIM* algorithm for monotonic dependencies, as this is an important class of dependencies as observed in Fig. 20. Additionally, a more computationally efficient algorithm to count the number of overlapping points for the hybrid case in Algorithm 2 could be researched.

From a copula theory and Markov chain perspective, the instability of the W copula, the stability of the Π copula, and the “apex” nature of the M copula as discussed in Appendix B should be further investigated. One area of research here is to understand the speed of convergence to maximum entropy, represented by the Π copula, when the Markov chain is time-homogeneous and non time-homogeneous. Additionally, it is well known that the W copula is not a valid copula for $D \geq 3$, where D is the dimensionality of the copula. This seems to correspond loosely to the n -fold Markov product of W corresponding to either W or M depending on whether n is even or odd, and this link should be further investigated.

Another area of research that will be conducted is to extend *CIM* to a measure of conditional dependence. By the invariance property of copulas to strictly increasing transforms (Embrechts et al., 2001), we can readily state that if $\{\mathbf{Y} \perp\!\!\!\perp \mathbf{Z}\}|\mathbf{X}$, then $\{\mathbf{V} \perp\!\!\!\perp \mathbf{W}\}|\mathbf{U}$, where $\mathbf{U} = (U_1, \dots, U_d) = (F_{X_1}(x_1), \dots, F_{X_d}(x_d))$, $\mathbf{V} = (V_1, \dots, V_k) = (F_{Y_1}(y_1), \dots, F_{Y_k}(y_k))$, and $\mathbf{W} = (W_1, \dots, W_n) = (F_{Z_1}(z_1), \dots, F_{Z_k}(z_n))$, and \mathbf{X} , \mathbf{Y} , and \mathbf{Z} are random vectors of arbitrary dimensionality. Due to the invariance property, conditional independence (and dependence) can be measured with the pseudo-observations. Using techniques from partial correlation, linear regression in each identified region of monotonicity can be computed. Similar to partial correlation, the residuals from this processing can then be compared for dependencies to create a measure of conditional dependence. Initial results have shown promising results for this application of *CIM*.

Acknowledgments

We would like to acknowledge the Hume Center at Virginia Tech for its support.

Appendix A. Proof of Theorem 1

Proof Let X and Y be two random variables such that X and Y are associated through the mapping $g(\cdot)$. Additionally, let Ω be the range-space of $(X, Y) \in \mathcal{R}^2$. Partition the sample space Ω into subspaces Ω_i , where each Ω_i corresponds to a monotonic section of the range space of (X, Y) . The partition of the sample space implies that $\bigcup_i \Omega_i = \Omega$, $\Omega_i \cap \Omega_j = \emptyset \forall i \neq j$. Define the random variable $X_i = X(\Omega_i)$. Additionally, define

$$\forall i, \quad g_i(x) = \begin{cases} g(x) & \forall x \in X_i \\ 0 & \text{otherwise} \end{cases}$$

$\therefore g(x) = \sum_{i=1}^n g_i(x)$. We can then write

$$\begin{aligned} F_Y(y) &= P(Y \leq y) \\ &= P(g(X) \leq y) && \text{(by substitution)} \\ &= \sum_i P(g_i(X_i) \leq y) P(X_i | X) && \text{(by Law of Total Probability)} \end{aligned}$$

Additionally,

$$\begin{aligned} P(g_i(X_i) \leq y) &= P(X_i \leq g_i^{-1}(y)) \\ &= \begin{cases} F_{X_i}(g_i^{-1}(y)) & \text{if } g_i^{-1}(y) \text{ is increasing} \\ 1 - F_{X_i}(g_i^{-1}(y)) & \text{if } g_i^{-1}(y) \text{ is decreasing} \end{cases} \\ &= \begin{cases} 1 & \text{if } x_i \geq K_i \\ 0 & \text{else} \end{cases} \quad \text{if } X_i = K_i \end{aligned}$$

where K_i is a constant.

$$g_i^{-1}(y) = g_i^{-1}(g(x)) = x_i \implies F_{X_i}(g_i^{-1}(y)) = F_{X_i}(x_i)$$

where $x_i \in X_i$. From the definition of conditional probability, we have that $P(g_i(X_i) \leq y) = \frac{F_X(x)}{P(X_i | X)} \quad \forall x \in X_i$ due to $P(X_i \cap X_j) = 0$. Because $F_{X_i}(x_i)$ and $F_X(x)$ are proportional to each other by the constant $P(X_i | X)$, and $F_{X_i}(x_i) = F_{X_i}(g_i^{-1}(y)) = F_Y(y)$, $F_Y(y)$ is a piecewise linear function of $F_X(x)$. ■

Appendix B. Proof of Theorem 2

Proof

We begin by proving that although τ does not satisfy DPI, $|\tau|$ does. To show this, we exploit the relationship between copulas and Markov chains initially presented by Darsow et al. (1992), and the ability to express any copula as a convex combination of its Fréchet-Hoeffding bounds on patches of the unit-square (Yang et al., 2006; Zheng et al., 2011). Another crucial property of copulas that we rely on for this proof comes from the 5th

property of concordance, which states that if $C_1 \preceq C_2$, then $\kappa(C_1) \leq \kappa(C_2)$, where κ is a measure of concordance (Scarsini, 1984). Using these three elements, we show that $C_{XY} \succeq C_{XZ}$ when $C_{XZ} \succeq \Pi$, which completes the proof that $|\tau|$ satisfies the DPI. Note that considering the set of copulas $\{C : C \succeq \Pi\}$ is equivalent to computing the absolute value of any measure of concordance. This is due to the fact that if a copula C_1 has a negative concordance τ_1 , (i.e. $C_1 \preceq \Pi$), then we can define $C_2(u, v) = C_1(v, u)$, where $\tau_2 = |\tau_1|$, implying that $C_2 \succeq \Pi$.

From Darsow et al. (1992), if X , Y , and Z follow a Markov Chain $X \rightarrow Y \rightarrow Z$, then $C_{XZ}(u, v) = C_{XY}(u, v) * C_{YZ}(u, v) = \int_0^1 \frac{\partial C_{XY}(u, t)}{\partial t} \frac{\partial C_{YZ}(t, v)}{\partial t} dt$. Using this, we would like to show that $|\tau(C_{XZ})| \leq |\tau(C_{XY})|$. From the 5th property of concordance, this is equivalent to showing that $C_{XZ} \preceq C_{XY}$, with the condition that $C_{XY}, C_{XZ} \succeq \Pi$. From Zheng et al. (2011), we can decompose a copula C as the convex combination of the Fréchet-Hoeffding lower and upper bounds, W and M respectively, and the independence copula Π , on patches of the unit-square. Decomposing C_{YZ} , we have

$$\begin{aligned} C_{YZ}(u, v) &= \sum_{i=0}^{m-1} \sum_{j=0}^{m-1} p_{ij} [\alpha_{ij} M^{ij}(u, v) + \beta_{ij} \Pi^{ij}(u, v) + \gamma_{ij} W^{ij}(u, v)] \\ \implies \frac{\partial C_{YZ}(t, v)}{\partial t} &= \sum_{i=0}^{m-1} \sum_{j=0}^{m-1} p_{ij} \left[\alpha_{ij} \frac{\partial M^{ij}(t, v)}{\partial t} + \beta_{ij} \frac{\partial \Pi^{ij}(t, v)}{\partial t} + \gamma_{ij} \frac{\partial W^{ij}(t, v)}{\partial t} \right] \end{aligned}$$

where $\alpha_{ij} + \beta_{ij} + \gamma_{ij} = 1$ and $\sum_{i=0}^{m-1} \sum_{j=0}^{m-1} p_{ij} = 1$. Substituting, we get

$$\begin{aligned} C_{XZ}(u, v) &= C_{XY} * C_{YZ}(u, v) = \int_0^1 \frac{\partial C_{XY}(u, t)}{\partial t} \frac{\partial C_{YZ}(t, v)}{\partial t} dt \\ &= \sum_{i=0}^{m-1} \sum_{j=0}^{m-1} \left[\alpha_{ij} \int_0^1 \frac{\partial C_{XY}^{ij}(u, t)}{\partial t} \frac{\partial M^{ij}(t, v)}{\partial t} dt + \beta_{ij} \int_0^1 \frac{\partial C_{XY}^{ij}(u, t)}{\partial t} \frac{\partial \Pi^{ij}(t, v)}{\partial t} dt \right. \\ &\quad \left. + \gamma_{ij} \int_0^1 \frac{\partial C_{XY}^{ij}(u, t)}{\partial t} \frac{\partial W^{ij}(t, v)}{\partial t} dt \right] \\ &= \sum_{i=0}^{m-1} \sum_{j=0}^{m-1} [\alpha_{ij} [C_{XY}^{ij} * M^{ij}] + \beta_{ij} [C_{XY}^{ij} * \Pi^{ij}] + \gamma_{ij} [C_{XY}^{ij} * W^{ij}]] \end{aligned}$$

From Darsow et al. (1992), we have that $C * M = C$, $C * \Pi = \Pi$, and $C * W(u, v) = u - C(u, 1 - v)$. From here on, for clarity of exposition, we omit the indices ij and the notation below is implied for each patch. Substituting these relations, we get

$$C_{XZ} = \alpha C_{XY} + \beta \Pi + \gamma [u - C_{XY}(u, 1 - v)]$$

Due to the 2-increasing property of copulas and $\alpha + \beta + \gamma = 1$, we can say that for each patch, $C_{XY} \succeq C_{XZ} \implies C_{XY} \succeq \alpha C_{XY}$, and $C_{XY} \succeq \Pi \implies C_{XY} \succeq \beta \Pi$. Additionally, by

assumption, we have

$$\begin{aligned}
C_{XY} \succeq \Pi &\implies C_{XY}(u, v) \geq \Pi(u, v) \ \forall u, v \in \mathbf{I} \\
&\implies C_{XY}(u, 1-v) \geq \Pi(u, 1-v) \\
&\implies C_{XY}(u, 1-v) \geq u - \Pi(u, v) \\
&\implies C_{XY}(u, 1-v) \geq u + (-\Pi(u, v)) \\
&\implies C_{XY}(u, 1-v) \geq u + (-C_{XY}(u, v)) \\
&\quad (\text{because } C_{XY}(u, v) \geq \Pi(u, v) \text{ implies } -C_{XY}(u, v) \leq -\Pi(u, v)) \\
&\implies C_{XY}(u, v) \geq u - C_{XY}(u, 1-v) \\
&\implies C_{XY} \succeq C_{XY} * W \\
&\implies C_{XY} \succeq \gamma(C_{XY} * W)
\end{aligned}$$

Thus, $C_{XY} \succeq C_{XZ}$ with the constraint that $C_{XZ} \succeq \Pi$ for every patch, and because we have a convex combination of patches and increasing the number of patches, m , decreases the approximation error to an arbitrarily small amount, it follows that $|\tau|$ satisfies DPI. We now use this result to show that *CIM* satisfies the DPI.

As seen in (10), *CIM* constructs a copula for each region of concordance and discordance, and computes the absolute value of Kendall's τ for each of these regions. Thus, to show that *CIM* satisfies DPI, we first show that for random variables X , Y , and Z that follow a Markov Chain $X \rightarrow Y \rightarrow Z$, if the domain of X is subdivided into disjoint sets X_i , then the associated Y_i and Z_i random variables (according to the Markov Chain, X is the cause of Y and Z , and hence Y_i and Z_i are associated with X_i) also satisfy DPI.

Define subsets of X as X_i , such that $\bigcup_i X_i \in X$ and $X_i \cap X_j = \emptyset \forall i \neq j$, then

$$\begin{aligned}
f_{X_i, Y_i}(x_i, y_i) &= \frac{f_{XY}(x, y)}{f_{X_i|X}(x_i|x)} \\
f_{X_i, Z_i}(x_i, z_i) &= \frac{f_{XZ}(x, z)}{f_{X_i|X}(x_i|x)}
\end{aligned}$$

Recall that because X , Y , and Z satisfy DPI, the relation

$$\int_Y \int_X f_{XY}(x, y) \log \left(\frac{f_{XY}(x, y)}{f_X(x)f_Y(y)} \right) dx dy \geq \int_Z \int_X f_{XZ}(x, z) \log \left(\frac{f_{XZ}(x, z)}{f_X(x)f_Z(z)} \right) dx dy$$

holds. Additionally, $f_{X_i|X}(x_i|x)$ is a constant. Hence, the following must hold:

$$\begin{aligned}
& \int_Y \int_X \frac{f_{XY}(x, y)}{f_{X_i|X}(x_i|x)} \log \left(\frac{f_{XY}(x, y)}{f_{X_i|X}(x_i|x)f_X(x)f_Y(y)} \right) dx dy \geq \\
& \quad \int_Z \int_X \frac{f_{XZ}(x, z)}{f_{X_i|X}(x_i|x)} \log \left(\frac{f_{XZ}(x, z)}{f_{X_i|X}(x_i|x)f_X(x)f_Z(z)} \right) dx dz \\
\implies & \int_{Y_i} \int_{X_i} f_{X_i Y_i}(x_i, y_i) \log \left(\frac{f_{X_i Y_i}(x_i, y_i)}{f_{X_i}(x_i)f_{Y_i}(y_i)} \right) dx_i dy_i \geq \\
& \quad \int_{Z_i} \int_{X_i} f_{X_i Z_i}(x_i, z_i) \log \left(\frac{f_{X_i Z_i}(x_i, z_i)}{f_{X_i}(x_i)f_{Z_i}(z_i)} \right) dx_i dz_i \\
\implies & X_i \rightarrow Y_i \rightarrow Z_i \\
\implies & C_{X_i, Y_i} \succeq C_{X_i, Z_i} \\
\implies & |\tau(X_i, Y_i)| \geq |\tau(X_i, Z_i)|
\end{aligned}$$

From the above, because X_i , Y_i , and Z_i is shown to satisfy the DPI, we can say that

$$\begin{aligned}
\sum_i w_i |\tau(X_i, Y_i)| & \geq \sum_i w_i |\tau(X_i, Z_i)| \\
\implies CIM(X, Y) & \geq CIM(X, Z)
\end{aligned}$$

because $\sum_i w_i = 1$. ■

We briefly note some interesting observations about the relationship between Markov Chains and copulas. From Lagerås (2010), it is known that if the Markov chain $X_0 \rightarrow X_1 \rightarrow \dots \rightarrow X_n$ is time-homogeneous and C is the copula for (X_0, X_1) , then the copula for (X_0, X_n) is given by C^{*n} , which is defined as the n -fold Markov product of C with itself. It is then shown in Chotimodum et al. (2014) that if $\alpha + \gamma < 1$ in the decomposition specified above, $\lim_{n \rightarrow \infty} C^{*n} = \Pi$. We have shown above that even in the non time-homogeneous case, that the copula between variables that are further apart in the Markov chain are “smaller” than copulas closer together. Returning to the time-homogeneous case, it is interesting to also note that the W is an unstable copula, as $\lim_{n \rightarrow \infty} W^{*n} = W$ if n is odd, and $\lim_{n \rightarrow \infty} W^{*n} = M$ if n is even. Finally, M is somewhat of an “apex” copula, and the only way to maintain this perfect dependence is to compute the Markov product with M .

Appendix C. Real-world Data Experiments Details

Real-world data analyzed for the monotonicity results shown above in Fig. 20 was derived from online sources.

C.1 Gene Expression Data

The gene expression related data was downloaded from the Broad Institute at the URL: <http://portals.broadinstitute.org/cgi-bin/cancer/datasets.cgi>. The enumeration below lists the specific files which were downloaded from the URL provided above (all with the .gct extension).

1. ALL	14. glioma_classic_hist	27. mLung
2. beer_lung_for_p53	15. glioma_nutt_combo	28. Multi_A
3. Breast_A	16. hep_japan	29. Multi_B
4. Breast_B	17. HL60	
5. Children_NE	18. HSC_FDR002	30. Normals_Leu
6. Common_miRNA	19. Iressa_Patient1_ams	31. Novartis_BPLC.top1000
7. crash_and_burn	20. leuGMP	32. PDT_miRNA
8. DLBCL_A	21. leukemia.top1000	33. Rap3hour_control
9. DLBCL_B	22. lung_datasetB_outcome	34. Rap24hour_control
10. DLBCL_C	23. LungA_1000genes	35. Res_p0005
11. DLBCL_D	24. met	36. Sens_p001
12. Erythroid	25. miGCM_218	37. Sens_p0005
13. GCM_All	26. MLL_AF9	
38. medullo_datasetC_outcome	40. med_macdonald_from_childrens	
39. lung_ann Arbor_outcome_only	41. megamiR_data.normalized.log2.th6	
42. Myeloid_Screen1_newData_021203_ams. AML_poly_mono		
43. Sanger_Cell_Line_project_Affymetrix_QCed_Data_n798		

The files, natively in GCT format, were stripped of metadata and converted to CSV files, and scanned for significant dependencies ($\alpha < 0.05$). The number of regions for the significant dependencies were then counted to determine the number of monotonic regions. The script to perform the conversion from GCT to CSV is provided at: <https://github.com/stochasticresearch/depmeas/tree/master/test/python/gcttocsv.py>. Additionally, the Matlab scripts to process the pairwise dependencies and produce the monotonicity results is provided at: https://github.com/stochasticresearch/depmeas/tree/master/test/analyze_cancerdata.m.

C.2 Financial Returns Data

The financial returns related data was downloaded from both finance.yahoo.com and Investing.com. We query the web API of these websites to download all available historical data (from Jan 1985 - Jan 2017) for the following indices:

1. A50	10. FTSE	19. KSE	28. SPTSX
2. AEX	11. GDAXI	20. MICEX	29. SSEC
3. AXJO	12. GSPC	21. MXX	30. SSMI
4. BFX	13. HSI	22. NK225	31. STOXX50E
5. BSESN	14. IBEX	23. NSEI	32. TA25
6. BVSP	15. ITMIB40	24. OMXC20	33. TRC50
7. CSE	16. IXIC	25. OMXS	34. TWII
8. DJI	17. JKSE	26. PSI20	35. US2000
9. FCHI	18. KOSPI	27. SETI	36. XU100

Less than 1% of the downloaded data was missing. In order to ease processing, missing data fields were imputed with the last known index price. The first difference of the stock prices was calculated in order to derive the returns data. The returns data was first determined to be stationary by the Dickey-Fuller test. After these procedures, pairwise dependencies between coherently aligned time series were computed. Because different amounts of historical data were available for the various indices, only the subset of data which belonged to both time series was tested for a significant dependency.

The script to perform the missing data imputation and raw data normalization is provided at: <https://github.com/stochasticresearch/depmeas/tree/master/test/python/normalizeStocksFiles.py>. Additionally, the Matlab scripts to process the pairwise dependencies and produce the monotonicity results is provided at: https://github.com/stochasticresearch/depmeas/tree/master/test/analyze_stocksdata.m. Finally, the raw stocks data is provided at https://figshare.com/articles/Stocks_Data/4620325.

C.3 Climate Data

The climate data was downloaded from the following links:

1. <https://www.kaggle.com/uciml/el-nino-dataset>
2. <https://www.kaggle.com/sogun3/uspollution>
3. <https://tinyurl.com/berkeleyearth>

The El-Nino data was normalized by extracting the zonal winds, meridional winds, humidity, air temperature, and sea surface temperature data from the dataset. The code to extract these features, and all to be described features from other climate related datasets is provided at: <https://github.com/stochasticresearch/depmeas/tree/master/test/python/normalizeClimateFiles.py>. Because these datapoints were collected over multiple decades and large chunks of missing data existed, each chunk of contiguous data (with

respect to time) was analyzed separately. The script to identify these chunks and coherently compute pairwise dependencies after checking for stationarity is provided at: https://github.com/stochasticresearch/depmeas/tree/master/test/analyze_elnino.m.

The global land temperatures data was normalized by extracting the land temperature for each country over the available date ranges. Again, due to significant chunks of missing data, each chunk of contiguous data was analyzed separately. The script to identify these chunks and coherently compute pairwise dependencies after checking for stationarity is provided at: https://github.com/stochasticresearch/depmeas/tree/master/test/analyze_landtemperatures.m.

The US pollution data was normalized by extracting NO₂ Air Quality Indicators (AQI), O₃ AQI, SO₂ AQI, and CO AQI for each location over the available date ranges. Again, due to significant chunks of missing data, each chunk of contiguous data was analyzed separately. The script to identify these chunks and coherently compute pairwise dependencies after checking for stationarity is provided at: https://github.com/stochasticresearch/depmeas/tree/master/test/analyze_pollution.m.

References

M. Ahsanullah, V. Nevzorov, and M. Shakil. *An Introduction to Order Statistics*, volume 3. Atlantis Press, 2013.

T. Bedford and R. Cooke. Vines—a new graphical model for dependent random variables. *The Annals of Statistics*, 30(4):1031–1068, 08 2002. doi: 10.1214/aos/1031689016.

P. Bellot, C. Olsen, P. Salembier, A. Oliveras-Vergés, and P. Meyer. Netbenchmark: a bioconductor package for reproducible benchmarks of gene regulatory network inference. *BMC Bioinformatics*, 16(1):312, 2015. doi: 10.1186/s12859-015-0728-4.

M. Ben Hassine, L. Mili, and K. Karra. A Copula Statistic for Measuring Nonlinear Multivariate Dependence, 2016.

D. Bonett and T. Wright. Sample Size Requirements for Estimating Pearson, Kendall and Spearman Correlations. *Psychometrika*, 65(1):23–28, 2000.

Y. Chang, Y. Li, A. Ding, and J. Dy. A Robust-Equitable Copula Dependence Measure for Feature Selection. *Proceedings of the 19th International Conference on Artificial Intelligence and Statistics*, 2016.

R. Chotimodum, T. Santiwipanont, and S. Sumetkijakan. Asymptotic Dependence of Markov Chains joined by a Patched Fréchet Copula. *The Annual Pure and Applied Mathematics Conference*, 2014. doi: 10.13140/2.1.3638.5921.

T. Cover and J. Thomas. *Elements of Information Theory (Wiley Series in Telecommunications and Signal Processing)*. Wiley-Interscience, 2006.

G. Darbellay and I. Vajda. Estimation of the Information by an Adaptive Partitioning of the Observation Space. *IEEE Transactions on Information Theory*, 45(4):1315–1321, May 1999. doi: 10.1109/18.761290.

W. Darsow, B. Nguyen, and E. Olsen. Copulas and Markov Processes. *Illinois J. Math.*, 36(4):600–642, 12 1992.

M. Denuit and P. Lambert. Constraints on Concordance Measures in Bivariate Discrete Data. *Journal of Multivariate Analysis*, 93(1):40 – 57, 2005. doi: <http://dx.doi.org/10.1016/j.jmva.2004.01.004>.

G. Elidan. Copula Bayesian Networks. In *Advances in Neural Information Processing Systems 23*. Curran Associates, Inc., 2010.

P. Embrechts, Lindskog F., and McNeil A. Modelling Dependence with Copulas and Applications to Risk Management, 2001.

S. García, J. Luengo, Sáez J., López V., and Herrera F. A Survey of Discretization Techniques: Taxonomy and Empirical Analysis in Supervised Learning. *IEEE Transactions on Knowledge and Data Engineering*, 25:734–750, 2013.

C. Genest and J. Nešlehová. A Primer on Copulas for Count Data. *ASTIN Bulletin*, 2007.

D. Helsel and R. Hirsch. *Statistical Methods in Water Resources Techniques of Water Resources Investigations, Book 4, chapter A3*. U.S. Geological Survey, 2002. URL <http://pubs.water.usgs.gov/twri4a3>.

H. Joe. Multivariate concordance. *Journal of Multivariate Analysis*, 35(1):12 – 30, 1990. doi: [http://dx.doi.org/10.1016/0047-259X\(90\)90013-8](http://dx.doi.org/10.1016/0047-259X(90)90013-8).

K. Kandasamy, A. Krishnamurthy, B. Poczos, L. Wasserman, and J. Robins. Nonparametric von Mises Estimators for Entropies, Divergences and Mutual Informations. In C. Cortes, N. D. Lawrence, D. D. Lee, M. Sugiyama, and R. Garnett, editors, *Advances in Neural Information Processing Systems 28*, pages 397–405. Curran Associates, Inc., 2015.

K. Karra and L. Mili. Hybrid Copula Bayesian Networks. *Probabilistic Graphical Models 2016 - JMLR: Workshop and Conference Proceedings*, 2016.

M. Kendall. A New Measure of Rank Correlation. *Biometrika*, 30(1-2):81–93, 1938.

M. Kendall. The Treatment of Ties in Ranking Problems. *Biometrika*, 33(3):239–251, 1945.

J. Kinney and G. Atwal. Equitability, Mutual Information, and the Maximal Information Coefficient. *Proceedings of the National Academy of Sciences*, 111(9):3354–3359, 2014.

A. Kraskov, H. Stögbauer, and P. Grassberger. Estimating Mutual Information. *Phys. Rev. E*, 69, 2004. doi: 10.1103/PhysRevE.69.066138.

A. Lagerås. Copulas for Markovian Dependence. *Bernoulli*, 16(2):331–342, 05 2010.

D. Lopez-Paz, P. Henning, and B. Schölkopf. The Randomized Dependence Coefficient. In *Advances in Neural Information Processing Systems 26*. Curran Associates, Inc., 2013.

L. Madsen and D. Birkes. Simulating dependent discrete data. *Journal of Statistical Computation and Simulation*, 83(4):677–691, 2013. URL <http://dx.doi.org/10.1080/00949655.2011.632774>.

A. Margolin, I. Nemenman, K. Basso, C. Wiggins, G. Stolovitzky, R. Favera, and A. Califano. ARACNE: An Algorithm for the Reconstruction of Gene Regulatory Networks in a Mammalian Cellular Context. *BMC Bioinformatics*, 7(1):S7, 2006.

P. Meyer, K. Kontos, F. Lafitte, and G. Bontempi. Information-Theoretic Inference of Large Transcriptional Regulatory Networks. *EURASIP Journal on Bioinformatics and Systems Biology*, 2007.

R. Nelsen. *An Introduction to Copulas*. Springer-Verlag New York, 2006.

J. Nešlehová. On Rank Correlation Measures for Non-Continuous Random Variables. *Journal of Multivariate Analysis*, 98(3):544–567, 2007.

K. Pearson. Note on Regression and Inheritance in the Case of Two Parents. *Proceedings of the Royal Society of London*, 58:240–242, 1895.

H. Peng, F. Long, and C. Ding. Feature Selection Based on Mutual Information: Criteria of Max-Dependency, Max-Relevance, and Min-Redundancy. *IEEE Trans. Pattern Anal. Mach. Intell.*, 27(8):1226–1238, 2005.

A. Rényi. On Measures of Dependence. *Acta Mathematica Academiae Scientiarum Hungarica*, 10(3):441–451, 1959.

D. Reshef, Y. Reshef, H. Finucane, S. Grossman, G. McVean, P. Turnbaugh, E. Lander, M. Mitzenmacher, and P. Sabeti. Detecting Novel Associations in Large Data Sets. *Science*, 334(6062):1518–1524, 2011.

Y. Reshef, D. Reshef, P. Sabeti, and M. Mitzenmacher. Equitability, interval estimation, and statistical power. *arXiv preprint arXiv:1505.02212*, 2015.

M. Scarsini. On Measures of Concordance. *Stochastica*, 8(3):201–218, 1984.

B. Schweizer and A. Sklar. On nonparametric measures of dependence for random variables. *Studia Mathematica*, 1974.

N. Simon and R. Tibshirani. Comment on "detecting novel associations in large data sets" by reshef et al, science dec 16, 2011, 2014.

C. Spearman. The Proof and Measurement of Association between Two Things. *The American Journal of Psychology*, 15(1):72–101, 1904.

Z. Szabó. Information Theoretical Estimators Toolbox. *Journal of Machine Learning Research*, 15:283–287, 2014.

G. Székely, M. Rizzo, and N. Bakirov. Measuring and Testing Dependence by Correlation of Distances. *The Annals of Statistics*, 35(6):2769–2794, 12 2007.

F. Vandenbende and P. Lambert. Improved Rank-Based Dependence Measures for Categorical Data. *Statistics and Probability Letters*, 63(2):157–163, 2003.

J. Yang, S. Cheng, and L. Zhang. Bivariate Copula Decomposition in Terms of Comonotonicity, Countermonotonicity and Independence. *Insurance: Mathematics and Economics*, 39(2):267 – 284, 2006. doi: <http://dx.doi.org/10.1016/j.insmatheco.2006.02.015>.

Y. Zheng, J. Yang, and J. Huang. Approximation of Bivariate Copulas by Patched Bivariate Fréchet Copulas. *Insurance: Mathematics and Economics*, 48(2):246 – 256, 2011. doi: <http://dx.doi.org/10.1016/j.insmatheco.2010.11.002>.

Xiang-Wei Zhu, Shu-Shen Liu, Li-Tang Qin, Fu Chen, and Hai-Ling Liu. Modeling non-monotonic doseresponse relationships: Model evaluation and hormetic quantities exploration. *Ecotoxicology and Environmental Safety*, 89:130 – 136, 2013.